Technical Report
TR-15-06
April 2016

Models for Diffusion in Compacted Bentonite

Andrés Idiart
Marek Pękala

SVENSK KÄRNBRÄNSLEHANTERING AB

SWEDISH NUCLEAR FUEL
AND WASTE MANAGEMENT CO

Box 250, SE-101 24 Stockholm
Phone +46 8 459 84 00
skb.se

SVENSK KÄRNBRÄNSLEHANTERING

ISSN 1404-0344
SKB TR-15-06
ID 1478613
April 2016

Models for Diffusion in Compacted Bentonite

Andrés Idiart, Marek Pękala
Amphos[21] Consulting S.L.

Abstract

The KBS-3V concept of deep geological repositories for spent fuel in Sweden and Finland relies to a large extent upon the performance of compacted bentonite, a material that will be used as buffer surrounding the copper canisters. The suitability of compacted bentonite is based on their confining properties, i.e. an elevated swelling capacity, a very low permeability, and a large sorption capacity for certain species. Under these conditions, solute transport in water saturated clays occurs almost exclusively by diffusion, thus limiting the release of radionuclides in the event of a failure of the canister. Even though diffusion in compacted clay and bentonite has been intensively studied during the last three decades, there remain at present a number of controversial issues regarding a mechanistic representation of the underlying phenomena. These issues result, in most of the cases, from a lack of a well-establish and widely accepted nano-/micro-structural conceptual model of compacted bentonite at different dry densities and salinities. The applicability of currently available characterization techniques for the porosity distribution and nanostructure of compacted bentonite is limited as they often perturb the structure of the water saturated bentonite. As a result, reliable experimental results are difficult to come by and indirect evidence must be relied on to a large extent. In these systems, the validity of the fickian diffusion approach has been questioned in some cases, as it is shown to not correctly represent the diffusion of cations, anions and neutral species simultaneously. More complex mechanistic models have been proposed in the literature to explain experimental data, based on different conceptualizations of the pore space.

In this work, the results of the Alternative Buffer Material (ABM) field test at Äspö Hard Rock

Laboratory in Sweden have been used to evaluate the applicability of different models to explain experimental observations. In particular, available data on the cation exchanger composition and chloride concentrations in the different blocks have been used to evaluate the following models:

1) Single bulk porosity coupled to cation exchange reactions.

2) Single interlayer porosity Donnan equilibrium model.

3) Multi-porosity (interlayer, double layer, and free) model.

The models consider the effects of the high temperature conditions of the test and groundwater composition used for the artificial saturation of the column, as well as the block-specific physical and chemical characterization data (30 blocks of 11 different compacted bentonites were randomly distributed in the column). The results obtained confirm that the classical Fickian diffusion approach using a single total (bulk) porosity fails to predict the concentration of anions in the bentonite blocks (in this case chloride). On the other hand, this simple approach, if coupled to cation exchange reactions, explains fairly accurately the evolution of the cation exchanger composition of the different blocks.

The single interlayer porosity Donnan equilibrium model and the multi-porosity (three porosity types, assuming complete anion exclusion from the interlayer and double layer porewater) are both able to explain the observed chloride concentrations in the different bentonite blocks. On the other hand, the Donnan equilibrium model largely overestimates in all cases the calcium occupancy of the exchanger at the expense of underestimating the sodium and magnesium fractions.

In addition, scoping calculations of a theoretical setup relevant to the Performance Assessment calculations of radionuclide migration in the KBS-3V concept have been repeated using different diffusion models. The goal is to compare the diffusive fluxes of different models when using a best guess parameterization approach. In this case, different diffusion coefficients have been typically used for different species, depending on the charge of the ions. Despite their conceptual differences, the results indicate that the diffusive fluxes obtained with the different models compare relatively well, especially for anions, and to a lesser extent for cations.

Sammanfattning

KBS-3V systemet för geologisk förvaring av radioaktivt avfall i Sverige och Finland bygger delvis på funktionen hos kompakterad bentonit, ett material som är tänkt att användas som buffert runt kapslar av koppar. Valet av kompaterad bentonit är baserat på materialets tätande förmåga, som kännetecknas av ett högt svälltryck, en mycket låg hydraulisk permeabilitet och en stark sorptionsförmåga för vissa ämnen. Detta medför att transporten av lösta ämnen i en vattenmättad bentonit alltid kommer att domineras av diffusion och därigenom begränsas uttransporten av radioaktiva ämnen i ett fall med kapselskada. Även om diffusion i kompakterad lera och bentonit har studerats intensivt de senaste trettio åren så återstår några kontroversiella frågeställningar angående den mekanistiska representationen av de underliggande fenomenen. Ursprunget till dessa frågeställningar är, i de flesta fall, avsaknaden av en väletablerad och allmänt accepterad nano-/mikrostrukturell konceptuell modell för kompakterad bentonit vid olika torrdensiteter och salthalter. Tillämpligheten av tillgängliga tekniker för att bestämma porositetsfördelningen och nanostrukturen i kompakterad bentonit är begränsad eftersom teknikerna ofta stör stukturen i en vattenmättad bentonit. Detta medför att det är svårt att hitta direkta experimentella resultat och att utvärderingen till stor del får baseras på indirekta observationer. I den här typen av system har validiteten av Ficks lag ifrågasatts för vissa tillämpningar eftersom det har visat sig att den inte samtidigt kan hantera diffusionen av katjoner, anjoner och neutrala specier. I den vetenskapliga litteraturen har därför mer komplicerade mekanistiska modeller föreslagis för att förklara experimentella data och dessa är baserade på olika konceptualiseringar av porutrymmet i bentoniten.

I den här studien har resultat från Alternativa Buffert Material (ABM)-försöket i Äspölaboratoriet i Sverige använts för att utvärdera tillämpligheten hos olika modeller för att förklara experimentella observationer. Det är särskilt data från katjonbytarens sammansättning och kloridjonkoncentrationen i de olika blocken som har används för att utvärdera följande modeller:

1) Bulk enkelporositet kopplad med katjonbytesreaktioner.
2) Mellanskikts enkelporositet med Donnanjämvikt.
3) Multiporositet (mellanskikt, dubbellager ochh fri).

Modellerna hanterar effekterna av den förhöjda temperaturen i försöktet, sammansättningen av det grundvatten som användes för den konstgjorda bevätningen samt data från den blockspecifika fysikaliska och kemiska karaktäriseringen (30 block från 11 olika kompakterade bentoniter var slumpmässigt fördelade i försöket). Resultaten bekräftar att den klassiska modellen med Ficks lag baserad på en enkelporositet (bulk) inte klarar av att förutsäga koncentrationen av anjoner i blocken (klorid i det här fallet). I andra sidan lyckas den modellen, kopplad med jonbytesjämvikter, ganska väl med att beskriva sammansättningen av jonbytaren i de olika blocken.

Mellanskikts enkelporositet med Donnanjämviktmodellen och multiporositetsmodellen (tre porositeter och med förutsättningen att inga anjoner finns i porvattnet i mellanskikten och dubbellagren) kan båda beskriva den observerade kloridkoncentrationen i de olika bentonitblocken. Å andra sidan så överskattar Donnanmodellen kalciumförekomsten i jonbytaren och underskattar natrium och magnesium i samtliga fall.

Jämförande beräkningar av radionulidmigration i ett KBS-3V-koncept för ett typiskt fall har genomförts med de olika modellerna. Målet var att jämföra diffusiva flöden i ett med en bästa uppskattning på värdena av de relevanta transportparametrarna. Trots de konceptuella skillnaderna så visar resultaten att de diffusiva flödena beräknade med modellerna är relativt jämförbara. Detta gäller särskilt för anjoner och i något lägre utsträckning för katjoner.

Contents

1 Introduction

1.1 Background: ion diffusion in compacted bentonite

The KBS-3V concept of deep geological repositories for spent fuel in Sweden and Finland relies to a large extent upon the performance of compacted bentonite, a material that will be used as buffer surrounding the copper canisters. The suitability of compacted bentonite is based on their confining properties, i.e. an elevated swelling capacity, a very low permeability (minimizing or even eliminating advective transport), and a large sorption capacity for certain species. Under these conditions, solute transport in water saturated clays occurs almost exclusively by diffusion, thus limiting the release of radionuclides in the event of a failure of the canister.

Even though diffusion in compacted clay and bentonite has been intensively studied during the last three decades (e.g. Oscarsson 1994, Kato et al. 1995, Sato et al. 1995, Ochs et al. 2001, Bourg et al. 2003, Molera et al. 2003, Muurinen et al. 1985, 2004, 2007, Van Loon et al. 2007, Birgersson and Karnland 2009, Kozaki et al. 2010, Tournassat and Appelo 2011, Tachi and Yotsuji 2014 for compacted bentonites; Appelo and Wersin 2007, Appelo et al. 2010 for Opalinus clay in Switzerland; Bazer-Bachi et al. 2005, Jougnot et al. 2009 for Callovo Oxfordian clay in France; Cavé et al. 2010 for Ordovician shale in Canada), there remain at present a number of controversial issues regarding a mechanistic representation of the underlying phenomena. These issues result, in most of the cases, from a lack of a well-establish and widely accepted nano-/micro-structural conceptual model of compacted bentonite and clayey materials at different dry densities and salinities. At present, available characterization techniques of the porosity distribution and microstructure of compacted bentonite often induce some kind of alteration of the microstructure of water saturated bentonite.

In such high density porous media, with very small pore sizes (on the nanometre scale), the validity of the fickian diffusion approach has been questioned in some cases, as it is shown to not correctly represent the diffusion of cations, anions and neutral species simultaneously. The effective diffusion coefficient is shown to be dependent on the dry density of the material, as well as on the salinity (ionic strength) of the external solution. Laboratory experiments have repeatedly demonstrated that, all other factors being equal, the transport of cations is faster than that of neutral species, and even more so than the transport of anions (see e.g. Sato et al. 1992, Wersin et al. 2004). This behaviour is typically explained in terms of distinct tortuosity factors for cations, anions and neutral species due to overlapping of electrical double layers of clay minerals at high degrees of compaction (e.g. Bourg et al. 2003) – a phenomenon termed “anion exclusion”. The increased diffusivity of cations is sometimes also explained in terms of “surface diffusion” (Appelo and Wersin 2007). Therefore, more complex mechanistic models have been proposed in the literature to try to capture experimental observations. These models typically involve a much larger number of parameters than the traditional fickian diffusion models, and they are consequently more difficult to parameterize. It is the purpose of this study to discuss the validity of the different approaches and models that have been published. The general framework within which many of the formulations proposed in these models fall is presented. It relies upon a multicomponent diffusion formulation accounting for the electrochemical migration term (Nernst-Planck equations), and the calculation of the Donnan equilibrium in the pore system.

In compacted clays and bentonite, the electrical double layer balancing the negative charge of the bentonite surfaces may play an important role. In some cases these double layers may overlap, completely or partially excluding anions from the porous medium. Pore narrowing or blocking due to electric effects has different effect on cations, anions and neutral species. While cations and neutral species can still pass through the pore, anions may be forced to circumvent the obstruction. As a result, tortuosity factors for cations and neutral species are smaller than those for anions.

To model ionic transport in such porous media, some authors have proposed to consider 3 types of water in compacted bentonite (Bourg et al. 2003, Wersin et al. 2004): (1) Interlayer water (with only water and cations balancing the charge of the Tetrahedral-Octahedral-Tetrahedral layers of montmorillonite), (2) Diffuse double layer (containing an excess of cations to balance the charge of the clay surface, and (3) Bulk pore water (charge balanced). The proportion of each type of water depends on

a number of factors, such as the degree of compaction of the clay/bentonite, and the ionic strength of the pore solution.

The controversial issues about bentonite microstructure have been intensified during the last years due, at least in part, to the appearance of coupled THMC modelling, which needs or calls for consistent models for each physical and chemical process playing a role in compacted bentonite (see e.g. Arthur 2010, Savage 2012). The different diffusion models proposed in the literature may in some cases conflict with models that represent other processes in bentonite, such as swelling and freezing. A well accepted microstructural model should therefore be capable of representing all these relevant processes.

A recent review of the SR-Site supporting documentation for SSM (Apted and Arthur 2012) has evidenced the presence of conflicting views on the importance of the Donnan equilibrium in controlling the diffusion properties of the buffer and backfill materials. It states:

"One view holds that diffusion will be controlled both by ion exchange and by a Donnan equilibrium established between aqueous solutions occupying smectite interlayer spaces and an external solution (SKB, 2010d; Birgersson and Karnland, 2009). An opposing view maintains that in domains larger than those typically used in experimental through-diffusion cells, Donnan equilibria and anion exclusion are relatively unimportant and can be ignored in models of buffer/backfill geochemical evolution (Sena et al. 2010)."

And adds:

"These contrasting views appear to be fundamentally incompatible. If so, this is an issue that is particularly safety-relevant because the Donnan equilibrium is invoked by SKB as an important diffusion-controlled constraint on the swelling pressure (SKB, 2011, Section 10.3.9; SKB, 2010d, Section 3.5.8) and because swelling pressure is an overarching direct or indirect safety function indicator for both the buffer and backfill."

In this context, a review of the different diffusion models available in the literature and their implications for the assessment of radionuclides transport in the clay barriers seems as a necessary step.

1.2 Objectives and methodology

The objective of this work is to perform a qualitative evaluation of the significance of different diffusion-based approaches to correctly represent ionic transport in compacted bentonite. The comparison of the cost to perform such calculations over the benefit obtained when compared to a simple fickian diffusion model is also discussed.

First, some of the different approaches available in the literature have been critically reviewed and the general formulation for multi-porosity multi-component diffusion is presented. In addition, the performance of different diffusion models in compacted bentonite has been assessed by a set of scoping calculations.

Existing data on pore water and cation exchanger composition of the Alternative Buffer Materials (ABM) in-situ test (Svensson et al. 2011) and the LOT A2 field test (Karnland et al. 2009) is used to qualitatively and quantitatively evaluate the validity of different models. The feasibility and convenience of up-scaling these models to 3D buffer scale simulations is discussed together with an evaluation of the pros and cons (cost vs. benefit) of each approach.

2 Literature review

2.1 Nano-/Micro-structural models for compacted bentonite

Compacted bentonite is typically composed of montmorillonite (> 75 wt. %) and a number of accessory minerals of different size (quartz, calcite, gypsum, etc.). The swelling properties and the low permeability of bentonite rely upon high montmorillonite content. In compacted clays and bentonite, the pore sizes are typically very small (nanometre scale and smaller) so that the electrical double layer balancing the negative charge of the montmorillonite surfaces may play an important role. Depending on the degree of compaction (dry density) and the salinity of the solution (ionic strength), these double layers may overlap and partially exclude anions from the porous medium (e.g. Bourg et al. 2003). To model ionic transport in such systems, several authors have proposed to consider 2 and even 3 types of water in compacted bentonite (e.g. Bourg et al. 2003, Wersin 2003, Wersin et al. 2004, Muurinen et al. 2007). A classical schematic representation of bentonite microstructure has been proposed by Bradbury and Baeyens (2003), as shown in Figure 2-1, where the existence of three different types of water is also suggested:

- Free pore water: charge balanced aqueous solution of cations and anions.
- Interlayer water: contains water and cations (compensating the structural charge deficit of Tetrahedral-Octahedral-Tetrahedral, TOT, layers) between montmorillonite TOT layers. This water is supposed to be devoid of anions.
- Electrostatic double layer (EDL) water (between mineral surface and free water): contains water, cations and a small amount of anions. The excess of cations balance the remaining charge at the outer surface of the montmorillonite.

The proportion of each type of water is obviously not constant but depends on the degree of compaction of bentonite (represented by its dry density), the salinity of the solution, or the amount of accessory minerals. The estimation of the different proportions has been addressed by a number of researchers (e.g. Bourg et al. 2003, Bradbury and Baeyens 2002, Appelo and Wersin 2007, Tournassat and Appelo 2011) to ultimately estimate the diffusion of different anionic, neutral, and cationic species.

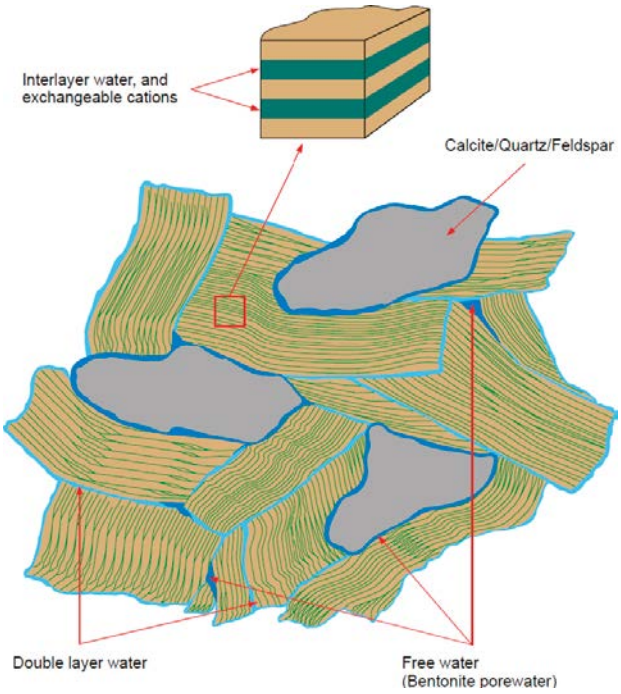

Figure 2-1. *Classical representation of compacted bentonite microstructure from Bradbury and Baeyens (2002).*

However, not only the proportions are important to estimate diffusive fluxes across a bentonite sample, but also how are these proportions distributed in the microstructure. Most of the models proposed in the literature disregard this effect by simply considering an additive representation of the diffusive fluxes across each porosity type, so that the total diffusive flux is the sum of all the different contributions. This is equivalent to assuming a diffusive model in parallel.

As also pointed by Jougnot et al. (2009), there is no reason to believe that bentonite microstructure should be ordered in such a parallel arrangement, which is as arbitrary as assuming a model in series for the three porosity types (which would yield substantially different results). Homogenization techniques (see e.g. Ponte Castañeda and Suquet 1998) are available that could be used to gain further insight into the effects of the microstructural distribution of each water type on the effective diffusive properties of compacted bentonite.

In their schematic model of compacted bentonite, Gimmi and Kosakowski (2011) consider a parallel model at the micro-scale, i.e. at the platelet scale, while they recognize that at the sample scale (macro-scale) the diffusion of species should occur not only in parallel but also in series (Figure 2-2). However, in their model it appears that the only effect of this distinction between a parallel representation and a combination of parallel-series units is that the tortuosity factor of the free pore water and the surface (or interlayer) water are identical. In that paper, it is not proved that this equality is representative of a model that combines parallel and series arrangement of clay particles. Another paper that recognizes this limitation has been published by Jougnot et al. (2009), where it is stated that electro-migration of the ions follows different paths between the bulk pore space and the surface of the pores.

The total porosity ϕ_{tot} of compacted bentonite can be calculated from the following expression:

$$\phi_{tot} = 1 - \frac{\rho_d}{\rho_s} \qquad \text{(Equation 2-1)}$$

where ρ_d is the dry density (kg · m^{-3}), i.e. the mass of clay (without hydration water) per unit total volume, and ρ_s (kg · m^{-3}) is the montmorillonite crystal density (grain density). This total porosity is composed of the contribution of free bulk water (ϕ_{free}), EDL water (ϕ_{EDL}), and interlayer water (ϕ_{IL}):

$$\phi_{free} + \phi_{EDL} + \phi_{IL} = \phi_{tot} \qquad \text{(Equation 2-2)}$$

A complete description of different microstructural models for anion exclusion in compacted bentonite has been presented elsewhere (Tournassat and Appelo 2011, Appelo 2013). A microstructural model for bentonite has been proposed in Tournassat and Appelo (2011), where the contribution of each porosity type to the total porosity is calculated from geometric considerations of montmorillonite sheets.

2.1.1 Interlayer porosity

The internal planar surface, $A_{planar,\,int}$ (m^2/kg), may be calculated as:

$$A_{planar,int} = 2 \cdot \frac{a \cdot b \cdot (n_c - 1)}{n_c} \cdot \frac{N_A}{M_w} \qquad \text{(Equation 2-3)}$$

where N_A is the Avogadro number, i.e. 6.02·1023, M_W is the molecular weight, a and b are the dimensions of the monoclinic unit cell in the horizontal plane, and n_c is the stacking number of TOT layers.

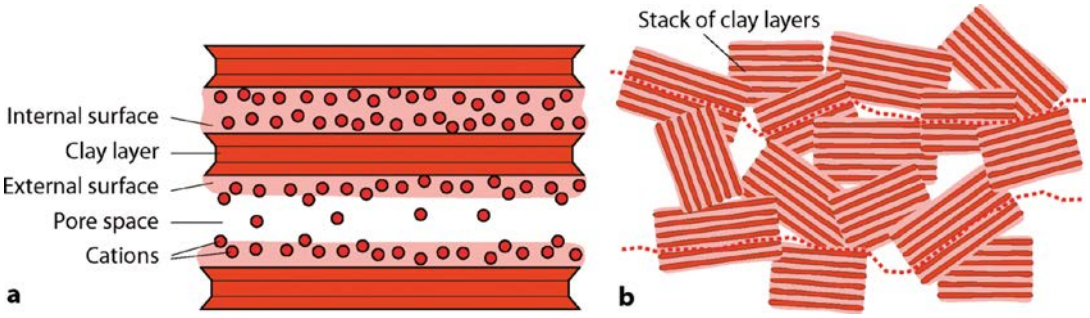

Figure 2-2. *Schematic representation of diffusion pathways in clays. (a) Local scale: Parallel pore and surface (including interlayer) diffusion. (b) Sample scale with several clay and possibly other particles: Diffusion in series through pore and surface regions (from Gimmi and Kosakowski 2011).*

The interlayer thickness, t_{IL} (m), can be calculated following the regression line proposed in Muurinen et al. (2007), who fitted different experimental data (Muurinen et al. 2004, Kozaki et al. 1997) with a linear relationship between IL thickness and dry density:

$$t_{IL} = 1.41 \cdot 10^{-9} - 4.9 \cdot 10^{-13} \cdot \rho_{dry} \qquad \text{(Equation 2-4)}$$

The volume of the interlayer (V_{IL}, m^3/kg) can then be calculated as (e.g. Appelo 2013):

$$V_{IL} = \frac{t_{IL} \cdot A_{planar,int}}{2} \qquad \text{(Equation 2-5)}$$

The interlayer porosity (ϕ_{IL}) then equals:

$$\phi_{IL} = V_{IL} \cdot f_{dens} \cdot w_{mm} \cdot \rho_{dry} \qquad \text{(Equation 2-6)}$$

where W_{mm} is the montmorillonite weight fraction and f_{dens} is the density ratio of water in the interlayer space and the free pore (not exactly known, used hereafter as 1). This expression is shown in Figure 2-3 for four different stacking numbers (n_c) as a function of dry density, and compared to the total porosity. It may be observed that for dry densities higher than ~1300 kg/m^3 (for all practical applications of bentonite) the interlayer porosity represents a very large fraction of the total porosity for stacking numbers (n_c) higher than 3.

2.1.2 Diffuse double layer: mean electrostatic potential

The Electrical Double Layer (EDL), or diffuse layer (DL), can be well approximated by a mean electrostatic potential (Donnan equilibrium). The thickness of the EDL depends on the ionic strength of the pore solution, so that its volume can be calculated from the external surface area of charged mineral (which can be measured using the BET method) multiplied by the diffuse layer thickness, t_{DDL} (m):

$$\phi_{DDL} = A_{ext} \cdot w_{mm} \cdot \rho_{dry} \cdot t_{DDL} \qquad \text{(Equation 2-7)}$$

in which A_{ext} ($m^2/kg_{dry\ bentonite}$) is the external surface area of montmorillonite, W_{mm} ($kg_{mont}/kg_{dry\ bentonite}$) is the weight fraction of montmorillonite in the bentonite, and ρ_{dry} ($kg_{dry\ bentonite}/m^3$) is the dry density. The diffuse layer thickness can be approximated by the Debye length κ^{-1} (distance over which the potential in the diffuse layer drops by e) multiplied by a constant:

$$t_{DDL} \cong \lambda \cdot \kappa^{-1} = \lambda \cdot \sqrt{\frac{3.94 \cdot 10^{-24} \cdot \varepsilon_r \cdot T}{I}} \qquad \text{(Equation 2-8)}$$

In the previous expression, I (mol/kgw) stands for the ionic strength of the pore solution, T is temperature (in Kelvin), ε_r (-) is the relative dielectric constant of water and the λ multiplier (-) represents the number of Debye lengths across the double layer thickness. Figure 2-4 shows the relation between the Debye length and the ionic strength. The important outcome of this is that the diffuse layer is significant only for diluted pore waters with low ionic strength, while it gradually vanishes for concentrated pore solutions.

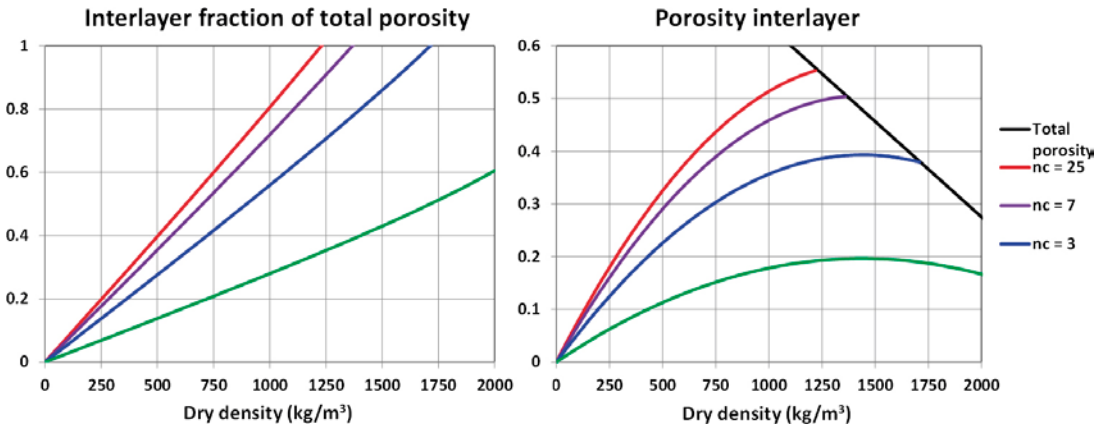

Figure 2-3. *Interlayer porosity as a function of the dry density (for different stacking numbers) according to Equations 2-3 to 2-6 (parameters used are shown in Table 3-7): as a fraction of total porosity (left) and interlayer porosity vs. total porosity.*

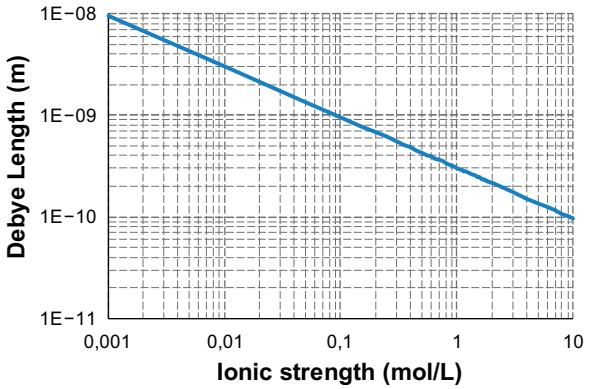

Figure 2-4. *Relation between the thickness of the double layer and the ionic strength.*

Equation 2-7 is plotted in Figure 2-5 for four different stacking numbers (n_c) as a function of dry density, and compared to the total porosity. It may be observed that only for dry densities higher than ~1500 kg/m^3 the DDL porosity represents a relevant fraction of the total porosity for stacking numbers (n_c) lower than 3 (which is not a representative value, see e.g. Pusch 2001).

The expression for A_{ext} (m^2/kg$_{\text{dry bentonite}}$) is (Tournassat and Appelo 2011):

$$A_{ext} = 2\frac{n_a n_c a \cdot c^* + n_b n_c b \cdot c^* + n_a n_b a \cdot b}{n_a n_b n_c}\frac{N_A}{M_w} \qquad \text{(Equation 2-9)}$$

The values of the external surface area for n_c = 1.5, 3, 7, and 25 are respectively 264, 135, 61, and 21 m^2/g, while typical values measured experimentally using BET(N_2) for MX80 bentonite range between 30 and 45 m^2/g (Bradbury and Baeyens 2002; Karnland 2010, Wersin et al. 2014). Note that during water saturation and homogenisation, the clay aggregates and stacks may broke thus increasing the external surface area (see Muurinen et al. 2007, for discussion).

2.1.3 Free (bulk) pore water

The volume of free water can be calculated from Equation 2-2 provided that the DDL and IL contributions to total porosity are known. Thus:

$$\phi_{free} = \phi_{tot} - (\phi_{EDL} + \phi_{IL}) \qquad \text{(Equation 2-10)}$$

Depending on the parameterization of the microstructural model presented above (Tournassat and Appelo 2011), the amount of free porosity may be very small or even negative, as shown in Figure 2-6, so that a minimum threshold value needs to be set in some calculation cases.

2.2 Ionic diffusion models: governing equations

Numerous models for diffusion of ions in compacted bentonite and clay-rocks have been proposed in the literature. Short and comprehensive reviews can be found in Bourg et al. (2003), Jougnot et al. (2009) or Appelo (2013). In recent years, empirical or semi-empirical diffusion models (e.g. Muurinen et al. 1988, Ochs et al. 2001, Van Loon et al. 2007) are being reviewed and gradually replaced by more sophisticated mechanistic models (e.g. Bourg et al. 2007, Appelo et al. 2010, Jougnot et al. 2009) that include our current understanding of the underlying processes.

In the following, the governing equations describing diffusion in compacted bentonite are presented in a format that is as general as possible. By simplification of this formulation, it would be then possible to obtain other models proposed in the literature. The conceptualization of the distribution of species within a single pore is approximately as depicted in Figure 2-7, where different layers between the charged mineral surface and the free electrolyte solution are observed. The ions in the Stern Layer and the protonation/deprotonation surface reactions can be calculated using a surface complexation model (either non-electrostatic or electrostatic). These ions are considered to be fixed, i.e. no diffusion. The diffuse layer is composed of mobile ions (mainly cations but also a small amount of anions) that balance the remaining charge of the mineral surface.

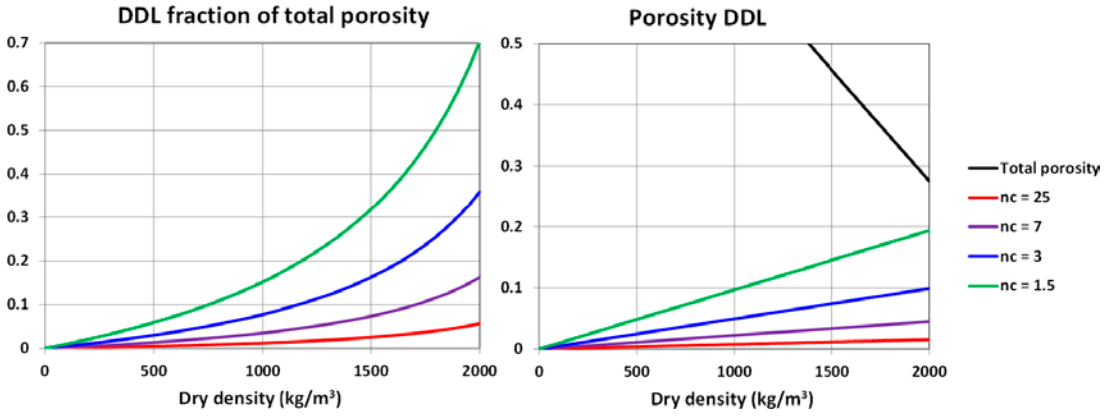

Figure 2-5. *Double layer porosity as a function of the dry density (for different stacking numbers) according to Equations 2-7 and 2-8 (parameters used are shown in Table 3-7): as a fraction of total porosity (left) and DDL porosity vs. total porosity.*

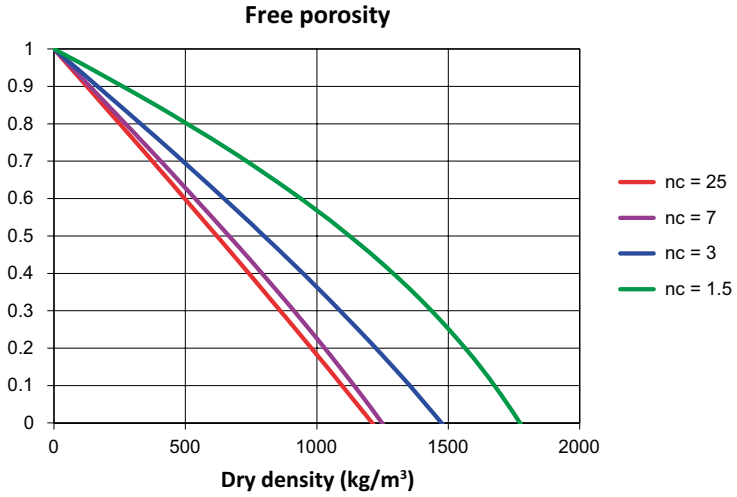

Figure 2-6. *Free or bulk porosity as a function of the dry density (for different stacking numbers) according to Equation 2-10 (parameters used are shown in Table 3-7) as a fraction of total porosity.*

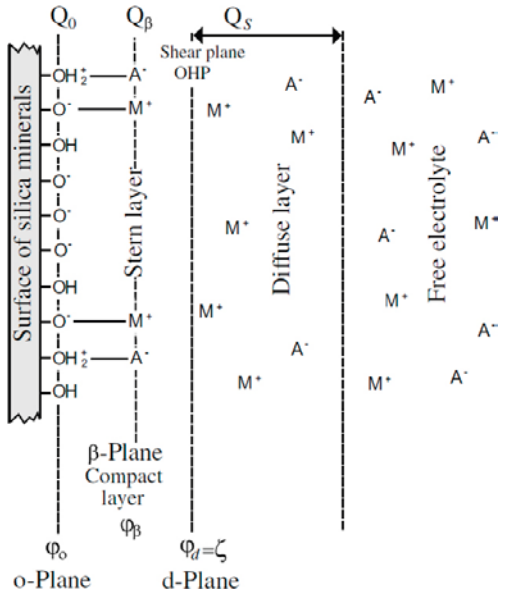

Figure 2-7. *Sketch of the electrical triple layer extending from the surface of the clay minerals to the centre of the pore. M^+ represents metal cations and A^- the anions (from Jougnot et al. 2009).*

For compacted bentonite at high dry densities, ionic transport through the interlayer water needs to be accounted for, since in some cases it may be dominant. In this scenario, such schematic representation of the pore structure is probably not valid. For any dry density envisaged for the bentonite buffer in a repository, there will be no free or bulk water in the interlayer space. The ability of anions to diffuse through the interlayer space is still controversial and no general agreement exists (see discussion above).

2.2.1 Electrochemical migration of ions: Nernst-Planck equations

Diffusion of charged species is rigorously represented by the Nernst-Planck system of equations, which includes the Coulombic coupling between ionic species (e.g. Samson et al. 1999, Snyder and Marchand 2001, Boudreau et al. 2004):

$$\phi \frac{\partial c_i}{\partial t} = \nabla \cdot \left(D_{e,i} \left(1 + \frac{\partial (ln\, \gamma_i)}{\partial (ln\, c_i)} \right) \nabla\, _i + \frac{D_{e,i} z_i F}{RT} \nabla \cdot c_i \nabla \varphi \right) \qquad \text{(Equation 2-11)}$$

in which c_i, γ_i (-) and z_i (-) are the concentration, the activity coefficient and valence of the ionic species i, respectively, ϕ is the total connected porosity, F is the Faraday constant (9.6485×10^4 C/mol), and R the ideal gas constant (8.3144 J/mol/K). The effective diffusion coefficient, $D_{e,i}$ (m^2/s), is defined for each species in the system (including all the aqueous complexes) in the following way:

$$D_{e,i} = \phi \cdot \tau \cdot D_{w,i} \qquad \text{(Equation 2-12)}$$

where $D_{w,i}$ (m^2/s) is the diffusion coefficient of species i in free solution (or self-diffusion coefficient), τ (-) is the overall tortuosity of the porous system ($0 < \tau < 1$). The overall tortuosity may be written in several ways:

– $\tau = \frac{\delta}{\theta^2}$, with δ the constrictivity (pore norrowing or widening) and θ^2 the tortuosity factor (which expresses how much longer is the path of a diffusing species with respect to the straight line); or:

– $\tau = \frac{1}{G}$, where G is the formation factor.

The tortuosity can be estimated from empirical relations such as the Archie's law $\tau = \phi^n$, where n is an empirical exponent that must be experimentally determined (typically ranges between 1 and 3).

The effective diffusion coefficient can also be expressed as a function of the different porosity types associated with bentonite microstructure: free (bulk) pore water, double layer water, and interlayer water (see e.g. Appelo 2013):

$$D_{e,i} = \frac{\phi_{free}}{\phi_{tot}} \cdot D_{e,i} + \frac{\phi_{DDL}}{\phi_{tot}} \cdot D_{EDL,i} + \frac{\phi_{IL}}{\phi_{tot}} \cdot D_{IL,i} \qquad \text{(Equation 2-13)}$$

where ϕ_{free}, ϕ_{DDL}, ϕ_{IL}, and ϕ_{tot} are the free (bulk), diffuse double layer (DDL), interlayer and total porosities, related by $\phi_{free} + \phi_{EDL} + \phi_{IL} = \phi_{tot}$, and $D_{e,i}$, $D_{EDL,i}$ and $D_{IL,i}$ are the effective diffusion coefficients within each type of porosity. In this way, different porosities and diffusion coefficients may result for different anionic and cationic species.

Solving the system of equations involves the calculation of an extra unknown, i.e. the electrical potential φ (V) that is locally induced in the electrolyte solution by the movement of all ionic species. To this end, an additional constraint is introduced to couple the transport of all ionic species to one another. The conservation of electroneutrality requires that the transport of all diffusing species should be coupled. During the diffusion process, some ions tend to diffuse at a higher rate. However, any excess charge transferred by the faster ions builds up a local electric field which slows down the faster ions, and reciprocally accelerates the slower ionic particles (Samson et al. 1999).

The additional constraint may be either the nil electrical current restriction, i.e.:

$$\sum_i z_i \cdot J_i = 0 \qquad \text{(Equation 2-14)}$$

or the nil net charge restriction (or electroneutrality condition, i.e. the net charge in every control volume is zero):

$$\sum_i z_i \cdot c_i = 0 \qquad \text{(Equation 2-15)}$$

A more rigorous constraint is to define the variation of the electric potential according to the spatial distribution of the electric charges, which is given by the Poisson equation (see e.g. Samson et al. 1999):

$$\nabla^2\varphi + \frac{\rho}{\varepsilon} = 0 \qquad \text{(Equation 2-16)}$$

where ε ($F \cdot m^{-1}$) is the permittivity of the medium and ρ is the electrical charge density ($F \cdot V \cdot m^{-3}$), which depends on the ionic concentrations in solution:

$$\rho = F\left(\sum_i z_i \cdot c_i + w\right) \qquad \text{(Equation 2-17)}$$

where w (mol/m^3) is a fixed charge density over the domain. Poisson equation can be simplified into the nil electrical current and nil net charge as special cases (e.g. Krabbenhøft and Krabbenhøft 2008).

A discussion on the effects of these different constraints on the transport of charged species is out of the scope of this report and may be found elsewhere (Boudreau et al. 2004; Samson et al. 1999, Krabbenhøft and Krabbenhøft 2008). It is generally found that for most practical cases these constraints lead to similar results. For instance, CrunchFlow (Steefel 2008) and PhreeqC (Parkhurst and Appelo 2013) use the nil electrical current condition (Equation 2-14) to calculate the potential, while e.g. Comsol Multiphysics uses the nil net charge condition (Equation 2-15).

The Nernst-Planck equation for multi-component diffusion can be used to calculate diffusive fluxes independently in each porosity type, i.e. the free water, the EDL water, and the interlayer water, as in geochemical codes PhreeqC and Crunchflow.

From a practical point of view, it is interesting to note that the cpu time needed to solve a given setup using the Nernst-Planck system of equations depends substantially on the amount of species transported, which includes all the charged and uncharged aqueous complexes in the system. Thus, the simulation time may be significant when numerous species are considered in the geochemical setup. Appendix A presents results of a simple 3D model of the Nernst-Planck equations using Comsol Multiphysics, where the dependence of the simulation time on the number of species, their charge, and the modelling approach (Fick's law or Nernst-Planck equations) is studied in detail. In most practical reactive transport applications, it is not expected that the cpu time needed for the transport step dominates over the time needed to solve the geochemical batch systems.

2.2.2 Charge balance condition for the EDL

Rigorously, solute concentration in the diffuse layer can be calculated explicitly by solving a combination of the Poisson-Boltzmann equation, an equation linking the surface charge with potential (e.g. based on the Guy-Chapman theory) and a charge balance equation. This can be done numerically (e.g. using the PhreeqC code) for an arbitrary system, but the operation is computer-intensive and often fails (Appelo and Wersin 2007). Alternatively, a simplified approach whereby an average composition of the diffuse layer is calculated based on the Donnan approximation (using a mean diffuse layer potential) can be used, which typically performs better in complex reactive transport simulations. Here the relation between the concentrations in the diffuse layer ($c_{i,DDL}$) and in the bulk solution (c_i) is given by the Boltzmann distribution (assuming the same activity coefficients in the bulk and double layer water, which may not be applicable, see e.g. Kraepiel et al. 1999; Bourg et al. 2003, Appelo and Wersin 2007, Leroy et al. 2007):

$$c_{i,DDL} = c_i exp\left(\frac{-z_i F \varphi_{DDL}}{RT}\right) \qquad \text{(Equation 2-18)}$$

where φ_{DDL} (V) is the mean potential in the double layer. To calculate the mean potential of the diffuse layer, an additional charge balance equation needs to be introduced that relates the concentration of each species in the double layer with the total charge in the Stern layer ($Q_{surface}$). This is given by:

$$\phi_{DDL}\sum_i z_i \cdot c_{i,DDL} + Q_{surface} = 0 \qquad \text{(Equation 2-19)}$$

In order to calculate $Q_{surface}$, a surface complexation model for cations (typically using the electrostatic model proposed by Dzombak and Morel 1990) needs to be coupled to the Donnan approximation of the diffuse layer. In this way, part of the total mineral charge is compensated in the Stern layer in the first hydration layer at the mineral surface (and also including protonation and deprotonation

reactions), while the rest of the charge is compensated by the diffuse layer (Tournassat and Appelo 2011, Jougnot et al. 2009, Steefel et al. 2010). Note that the Stern layer calculation includes a surface potential as an additional unknown when an electrostatic model is used (e.g. Steefel et al. 2010).

The model proposed by Leroy et al. (2007) and Jougnot et al. (2009) for CallOx considers that the charge of the surface can be calculated directly from the cation exchange capacity of the clay (CEC), without including the charge of the external surfaces that are not in contact with interlayer water. In the same spirit, Birgersson and Karnland (2009) consider that all the pore water is represented by interlayer water, and thus the charge balance condition is imposed also assuming the CEC as the charged surface. On the contrary, Appelo and Wersin (2007), Steefel et al. (2010) and Tournassat and Appelo (2011) calculate the surface charge of the external surfaces, not including the internal surfaces in contact with interlayer water.

2.2.3 Interlayer water: an additional diffusion path

As shown in Section 2.1, the interlayer porosity typically represents a large portion of the total porosity for most practical applications of compacted bentonite (dry densities larger than ~1300 kg/m^3). This has been measured experimentally (e.g. Holmboe et al. 2012) and interpreted from experimental results and from physical quantities (e.g. Bourg et al. 2003, 2007, Kozaki et al. 2008, 2010). It is now relatively well established that cations can diffuse through the interlayer water. Several diffusion experiments have measured this process (Glaus et al. 2007, 2013), while other researchers have proposed surface diffusion models to represent different experimental data-sets (e.g. Kato et al. 1995, Eriksen et al. 1999, Bourg et al. 2003, Gimmi and Kosakowski 2011).

In the case of anions, while most researchers agree that diffusion in the interlayer between montmorillonite layers is limited to cations, there are some recent publications where anions diffusion through the interlayer is suggested, based on ab-initio calculations (Hedström and Karnland 2012). Partial anion exclusion from the interlayer water is also assumed in some models that entirely rely upon Donnan equilibrium (Muurinen et al. 2007, Birgersson and Karnland 2009).

In the cases where interlayer diffusion is a relevant transport mechanism, the governing equation can be expressed as a function of the gradient of the unity fraction of the cation exchanger composition:

$$J_{IL,i} = -\phi_{IL} \cdot \tau \cdot D_{w,i} \cdot \frac{c_{IL,CEC}}{|z_i|} \nabla \beta_i \qquad \text{(Equation 2-20)}$$

Where β_i is the equivalent (unity) fraction of the exchangeable cation and $c_{IL,CEC}$ is the cation exchange capacity (CEC) expressed in mol/m^3 of interlayer water.

2.2.4 Diffusion models implemented in geochemical modules

The general formulation presented in the previous section has been implemented in at least two well-known geochemical codes, i.e. PhreeqC (Parkhurst and Appelo 2013) and Crunchflow (Steefel 2008, Steefel et al. 2010). A third code, MIN3P (Mayer et al. 2012), is currently in the implementation phase.

In addition to these processes, surface complexation (with or without electrostatic effects) and cation exchange reactions are also considered (see formulation in Parkhurst and Appelo 2013). Obviously, in these codes the coupling to kinetic and/or equilibrium reactions of the mineral precipitation/dissolution and aqueous speciation processes can be readily introduced in the model. The formulation for these reactions is standard and is out of the scope of this report. The reader is referred to e.g. the manuals of PhreeqC (Parkhurst and Appelo 2013) and Crunchflow (Steefel 2008).

A diffusion benchmark modelling test has been conducted by Amphos 21 to verify the similarities of the two implementations and whether important differences are found. The description of the benchmark and the results are presented in Appendix B. The two codes give essentially the same results in a case with several processes, such as multi-porosity, multi-component diffusion (Nernst-Planck equations), dynamic evolution of porosity distribution as a function of ionic strength, or surface complexation reactions.

Most models presented in the literature are implemented in a one-dimensional setup, whereas the use of such diffusion models to more complex experiments, such as the ABM, need at least two-

dimensional axisymmetric representation. In addition, multicomponent diffusion coupled to a double porosity microstructural representation is typically much more computationally demanding than the fickian diffusion models. These features need to be considered when evaluating the benefits versus cost of a given model.

Most of the geochemical speciation and reactive transport codes available rely on a formulation based on solute concentrations on the free porosity, from which everything else (mineral reactions, concentrations in the diffuse double layer, etc.) is calculated. Even though this formulation gives flexibility to calculate diffusion through compacted bentonite assuming different hypotheses (multi-porosity, dynamic and static partition of porosity between free and DDL, exchanger or interlayer porosity and diffusion), it is not suitable by definition to consider the case of overlapping diffuse double layers, where free porosity vanishes (which would be equivalent to the formulation proposed by Birgersson and Karnland 2009). Indeed, a small portion of free porosity needs to be present to perform the geochemical calculations. Moreover, the convergence of such geochemical codes may encounter problems in the cases of very small (or vanishing) free porosities.

2.2.5 Donnan equilibrium model (Birgersson and Karnland 2009)

The relatively slow anion diffusion in compacted bentonite has been traditionally interpreted as a reduced available porosity for anions. In contrast, Birgersson and Karnland (2009) proposed a model in which the low flux results from a concentration drop at the clay/external solution interface due to interlayer ion equilibrium. In their view, the interpretation of anion porosity as a volume restriction is not correct, although it may represent the Donnan equilibrium effect in a quantitatively (but not conceptually) correct manner.

It is argued by these authors that the use of continuous concentration profiles as boundary conditions has typically required the use of a multi-porosity model to correctly describe measured data. This need can be eliminated by the use of a Donnan equilibrium model, as proposed in Birgersson and Karnland (2009). This model considers solute diffusion in a single porosity (i.e. the interlayer water between montmorillonite sheets) compacted bentonite (Figure 2-8). As a consequence, diffusion of anions is assumed to occur entirely through this interlayer space, contrary to the traditionally assumed total anion exclusion from the interlayer (Wersin et al. 2004, Van Loon et al. 2007, Tournassat and Appelo 2011).

The formulation of the Donnan equilibrium model is derived from basic thermodynamics, i.e. from chemical potentials of the internal (μ_i^{int}) and external (μ_i^{ext}) solutions, to explain the concentration drop at the clay/solution interface, which is due to Donnan equilibrium:

$$\mu_i^{ext} = \mu_{0,i} + RT \cdot ln\left(a_i^{ext}\right) \quad \text{(Equation 2-21)}$$

$$\mu_i^{int} = \mu_{0,i} + RT \cdot ln\left(a_i^{int}\right) + F \cdot z_i \cdot \Delta\varphi \quad \text{(Equation 2-22)}$$

where a_i^{int} and a_i^{ext} are the activity of ion i in the internal and external solutions, respectively ($a_i^{int,ext} = \gamma_i^{int,ext} \cdot c_i^{int,ext}$, with $\gamma_i^{int,ext}$ the activity coefficient of the i-th ion in the internal or the external solution), F is the Faraday constant, z_i is the charge of the species i, and $\Delta\varphi$ is the mean (Donnan) potential in the interlayer. At equilibrium, the chemical potentials must be equal and therefore:

$$ln\left(\frac{a_i^{int}}{a_i^{ext}}\right) = -\frac{F \cdot z_i \cdot \Delta\varphi}{RT} \quad \text{(Equation 2-23)}$$

From this equation, an ion equilibrium coefficient, Ξ, may be defined as a function of the mean potential, φ (V), of the interlayer water:

$$\frac{a_i^{int}}{a_i^{ext}} = exp\left(-\frac{F \cdot z_i \cdot \Delta\varphi}{RT}\right) = \Xi^{-z_i} \quad \text{(Equation 2-24)}$$

$$\Xi = e^{\frac{F \cdot \varphi}{RT}} = e^{\frac{\pm e \cdot \varphi}{k_b T}} \quad \text{(Equation 2-25)}$$

In the above equations, c_i^{int}(mol/kgw) is the concentration of the ion i in the bentonite pore water, c_i^{ext} (mol/kgw) is the concentration of the ion i in the external solution, z_i is the charge of the ion i, F is the Faraday constant, k_b is the Boltzmann constant (1.381×10^{-23} J/K), R is the ideal gas constant, and T is temperature in Kelvin. Equations 2-26 and 2-27 give a set of expressions for all the ions present in solution from which the ion equilibrium coefficient may be calculated.

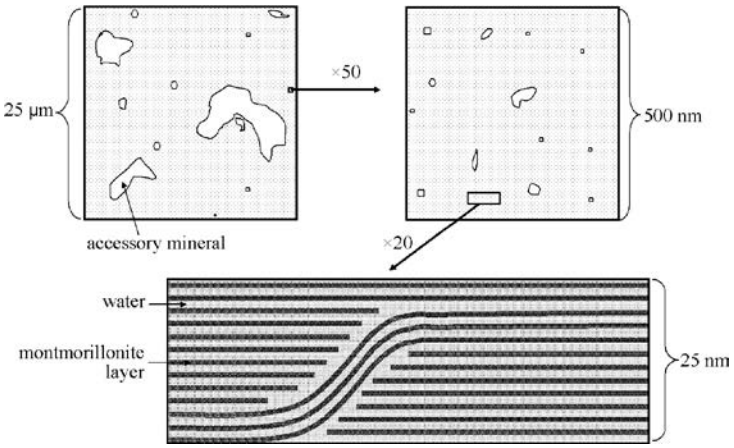

Figure 2-8. *Schematic representation of bentonite structure according to Birgersson and Karnland (2009).*

An additional constraint is added to fulfil charge balance (in terms of concentrations) of the system:

$$\sum c_i^{int} \cdot z_i = -\frac{Q_{clay}}{V_p} \equiv c_{IL} = \frac{CEC \cdot \rho_w}{w \cdot (1\frac{eq}{mol})} \qquad \text{(Equation 2-26)}$$

or:

$$\sum \Xi^{-z_i} \cdot c_i^{ext} \cdot z_i = c_{IL} \qquad \text{(Equation 2-27)}$$

where Q_{clay} and V_p are respectively the charge of the clay mineral surfaces and the pore volume, *CEC* (eq/kg dry clay) is the cation exchange capacity of the clay, ρ_w (kg/liter) is the water density, and *w* (kgw/kg dry clay) is the water content. c_{IL} (mol/kgw) is thus a measure of the charge of the interlayer solution.

To calculate diffusive fluxes at steady state, *J*, Birgersson and Karnland (2009) propose the simple expressions:

$$J = -D_e \cdot \nabla c_{ext} \qquad \text{(Equation 2-28)}$$

where $\nabla c_{ext} = -c_{ext}/L$, with *L* the diffusion length, and

$$D_e = \phi_c \cdot \Xi \cdot D_c \qquad \text{(Equation 2-29)}$$

In the above equation, D_c is equivalent to the pore diffusivity (or the apparent diffusivity if there is retardation), and the effect of filters (if used in experiments) is neglected. This was shown by these authors to be a valid assumption for chloride diffusion.

In this model, the fitting parameter is D_c, while the ion equilibrium coefficient can be calculated from the chemical composition of the internal and external solutions, as shown in Section 3.1.3. For chloride diffusion, the authors verified the model with the tracer experiments of Van Loon et al. (2007) and determined the relation:

$$D_e = \phi_c \cdot \Xi \cdot D_c = \phi_{Cl} \cdot D_c \qquad \text{(Equation 2-30)}$$

in which ϕ_{Cl} is the chloride available porosity measured by Van Loon et al. (2007). This implies that D_c has no or very weak dependence on external concentration (Birgersson and Karnland 2009).

2.2.6 Semi-empirical diffusion models

A number of semi-empirical approaches have been developed to model radionuclide diffusion in compacted bentonite. For example, Van Loon et al. (2007) studied the diffusion of $^{36}Cl^-$ in compacted bentonite using through-diffusion, out-diffusion and profile analysis techniques. Experiments were carried out on bentonite samples of varying dry density (1300, 1600, and 1900 kg/m^3) and ionic strength (0.01, 0.05, 0.1, 0.4, and 1 M). Based on their experimental results, they identified and

estimated two critical parameters: chloride accessible porosity and effective diffusion coefficient. The chloride accessible porosity was fitted to an exponential expression that depends on the ionic strength of the solution, I, in the following way:

$$\varepsilon_{Cl} = \varepsilon_{Cl}^{max} - A \cdot e^{-B \cdot I} \quad \text{(Equation 2-31)}$$

where A and B are fitting coefficients (fitted for three different values of the considered dry densities), and ε_{Cl}^{max} is identified as the inter-particle pore space.

Using a collection of previously published data the authors fitted the effective diffusion coefficient to the empirical formula (analogous to the Archie's law):

$$D_{e,Cl} = D_{w,Cl} \cdot \varepsilon_{Cl}^{n} \quad \text{(Equation 2-32)}$$

where $D_{w,Cl}$ is the free water diffusion coefficient and n is an empirical coefficient equal to 1.9±0.1. Using the two above formulae, the diffusive flux of Cl^- in compacted bentonite can be calculated as a function of the ionic strength of the pore water for bentonites compacted to dry densities of 1300, 1600 and 1900 kg/m^3.

Wersin et al. (2014) compiled currently available data on anion, cation and neutral species diffusion in compacted bentonite and derived empirical relations for the calculation of the effective diffusion coefficient as a function of bentonite dry density and temperature. They derived the following empirical expression for the effective diffusion coefficient of anions (D_e) in compacted bentonite as a function of the bentonite dry density (ρ_d) and ionic strength (I):

$$D_e = 3 \cdot 10^{-7} \cdot e^{-0.0066 \cdot \rho_d} \cdot I^{0.64(\pm 0.08)} \quad \text{(Equation 2-33)}$$

Ochs and Talerico (2004) presented an assessment and recommendation of key transport parameter (diffusion-available porosity, effective diffusivity and distribution coefficient) values for a total of 38 elements to be used in the prediction of radionuclide transport in compacted bentonite within the SR-Can Performance Assessment. The values were derived from a systematic review of available datasets in the literature and/or from thermodynamic models. The majority of these recommended values were later carried over and used in the SR-Site Performance Assessment (SKB 2010). These data were derived for conditions relevant to the prospective disposal and are hence conditional, e.g. evaluated for specific pore water composition, solid/water ratio and dry density of the MX-80 bentonite (1590 kg/m^3). The data presented in Ochs and Talerico (2004) can be used to calculate diffusive fluxes of relevant cations, anions and neutral species through the bentonite by multiplying the effective diffusion coefficient by the pertinent solute concentration gradient:

$$J_i = D_{e,i} \cdot \nabla c_i \quad \text{(Equation 2-34)}$$

where J_i, $D_{e,i}$, ∇c_i are respectively the steady state flux (mol $\cdot$ m^{-2} $\cdot$ s^{-1}), the effective diffusion coefficient, and the gradient of concentration of species i.

3 Scoping calculations

3.1 Revisiting ABM experimental data

3.1.1 Introduction and previous work

Even though MX-80 bentonite is the reference buffer material in the KBS-3V concept, SKB has also been investigating different alternatives (Svensson et al. 2011). In 2006, the field experiment Alternative Buffer Materials (ABM) was started at the Äspö Hard Rock Laboratory (HRL). Three packages, deposited into 3 meter deep boreholes, made of eleven different compacted bentonite materials arranged in different configurations were tested over varying time scales. After installation, packages were saturated and heated differently to target values.

The evolution of Package 1, which was initiated in December 2006 and ran for ~2.5 years, was studied using numerical modelling (Pękala et al. 2012), see Figure 3-1. Post-mortem examination after retrieval showed that the initially contrasting chloride concentrations and cation-exchanger compositions between different bentonite blocks became significantly homogenised (Svensson et al. 2011, Dohrmann et al. 2013). These observations have been later confirmed in the post-mortem examination of the Package 2, which has been recently dismantled, showing a similar pattern.

It has been argued that this behaviour could be explained as a first approximation by diffusion of major ions between the bentonite blocks coupled with cation-exchange. In previous work (Pękala et al. 2012), a modelling study to verify this hypothesis was undertaken. The behaviour of major cations (Na^+, Ca^{+2}, Mg^{+2}, and K^+) and the exchanger composition were studied in detail in Package 1. The model, implemented in the finite element software Comsol Multiphyics®, considered a two-dimensional axisymmetric representation of the depositional borehole. It included coupled diffusion and cation-exchange of Na^+, K^+, Ca^{+2}, and Mg^{+2} (as a chloride solution) in a stack of 30 bentonite blocks of 11 distinct initial compositions (Figure 3-1). Ion diffusion was allowed between individual bentonite blocks and also between the bentonite blocks and a sand layer filling the bentonite-rock gap. The effective diffusion coefficient values for individual bentonite blocks were estimated based on the dry density of the bentonite. The temperature-dependent evolution of the diffusion coefficients is approximated with an empirical relation (the heater increases the temperature of the package to about 100–130 °C).

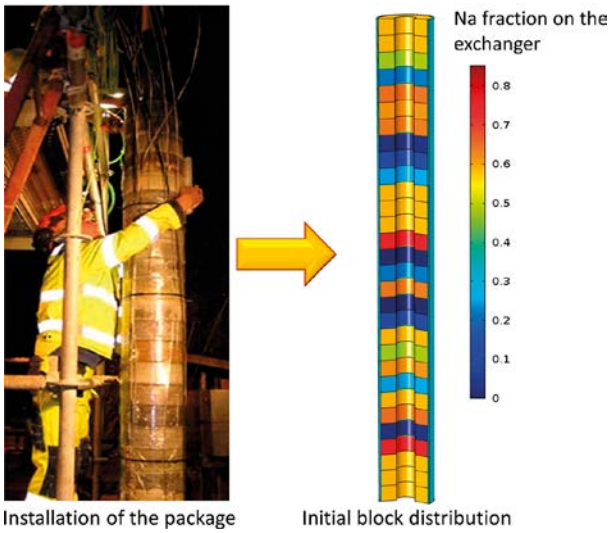

Figure 3-1. *Installation of the package and conceptualization in Comsol model.*

The model results indicated that the effect of diffusion on the cation exchange homogenisation for the studied cations is significant and has the potential to explain quantitatively the observed patterns in the package. This is specially the case for the dominant cations Ca^{+2} and Na^{+} (Figure 3-2). The boundary conditions surrounding the package obey qualitatively to the distribution of fractures in the bedrock (upper half more fractured than bottom half), see Figure 3-2. Typical results of the distribution of calcium in the cation exchanger of the column are shown in Figure 3-3.

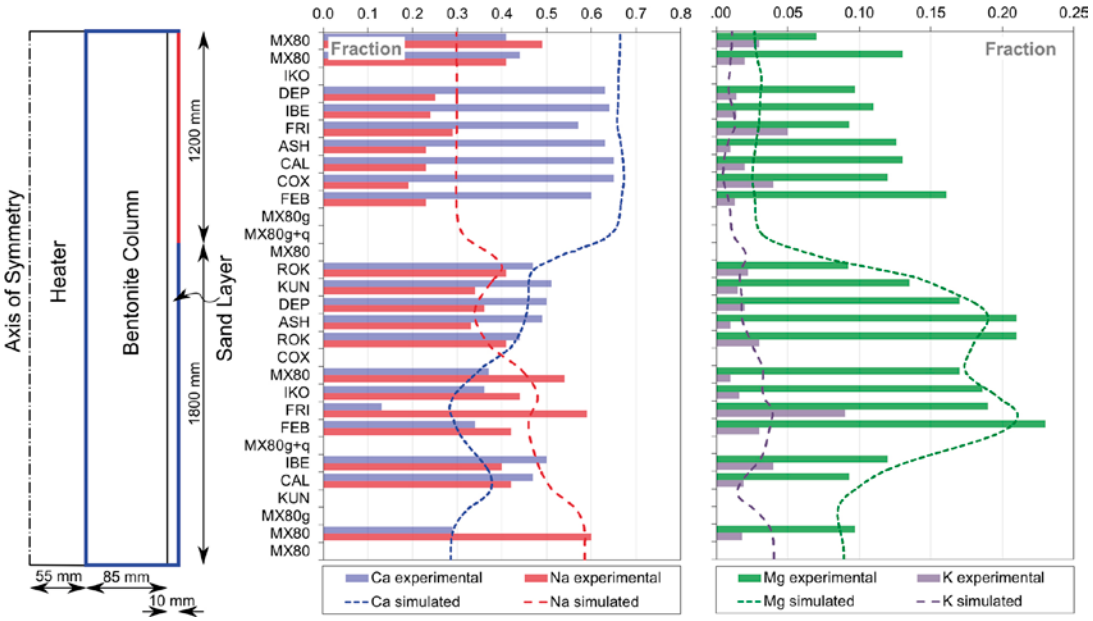

Figure 3-2. *Left – schematic representation and dimensions of the model domain and its boundaries (blue: no-flux, red: constant concentration). Right – experimental (bars) and calculated (dashed lines) counterion fractions in ABM Package 1, after dismantling at 880 days: Ca^{+2} and Na^{+} (left), and Mg^{+2} and K^{+} (right). Note the different scales in the horizontal axes in each plot.*

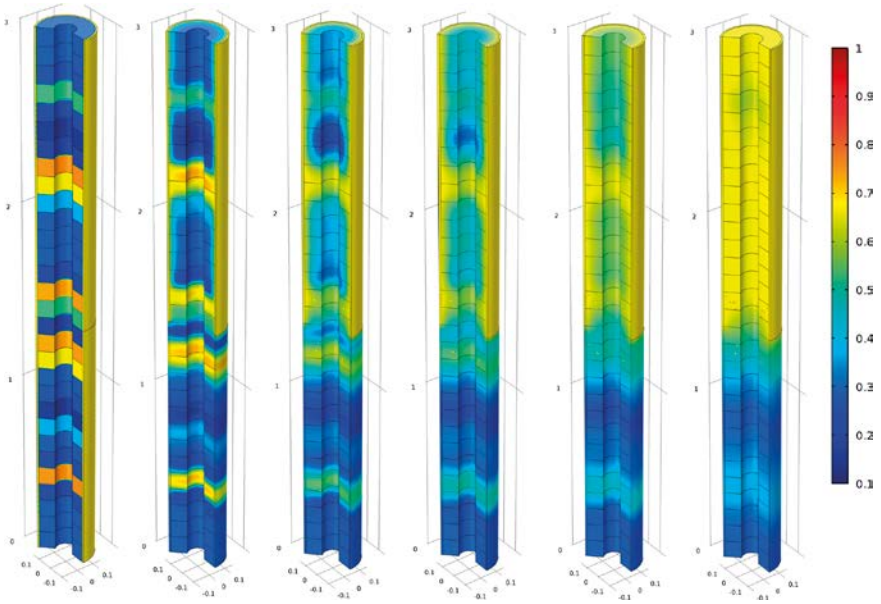

Figure 3-3. *Typical results of time evolution of Ca^{+2} unit fraction on the cation exchanger. From initial state (left) to final state – after 880 days (right).*

3.1.2 Diffusion of anions: the case of chloride

The transport of anions was not specifically addressed in the model developed by Pękala et al. (2012). In particular, available results of chloride diffusion in the different blocks (Svensson et al. 2011) were not interpreted or modelled. The relatively homogenous final chloride concentrations measured across the bentonite columns (where marked initial concentration contrasts were present) suggest that not only have chloride concentrations homogenised between individual bentonite blocks, but also with chloride concentrations in the boundary groundwater (Figure 3-5, left). In the model, chloride was used to charge balance the solution (the only anion present), and therefore the concentrations were not exactly the same as the measured values in groundwater and blocks. In any case, the Fick's diffusion model used (Pękala et al. 2012) predicts a chloride concentration in the blocks almost in equilibrium with the external water, with the same concentration in the open boundary (see Figure 3-2 left), as expected. This is shown in Figure 3-4. Therefore, it may be concluded that the single porosity Fick's diffusion model is not able to capture simultaneously the observed chloride concentrations and cation exchanger composition.

The anions of soluble salts (F^-, Cl^-, SO_4^{2-}, NO_3^-, PO_4^{3-}) were determined in water extracts of the bulk bentonite (Svensson et al. 2011). Initial (reference samples) and final (i.e. after the field test) chloride concentrations were measured for several blocks (Figure 3-5). Measured chloride contents (mass chloride per mass dry bentonite) were recalculated into molarity (moles of chlorite per litre of pore water).

The chloride profiles along the thickness of the blocks (Figure 3-6) indicate that the saturation with groundwater (composition given in Table 3-1) and subsequent diffusive transport resulted in laterally and vertically smoothed and approximately constant concentrations. Therefore, the most Cl-rich bentonites/clays (Asha 505, Friedland and Ikosorb) showed a decrease in chloride, whereas the other bentonites displayed an increase in chloride during the field test.

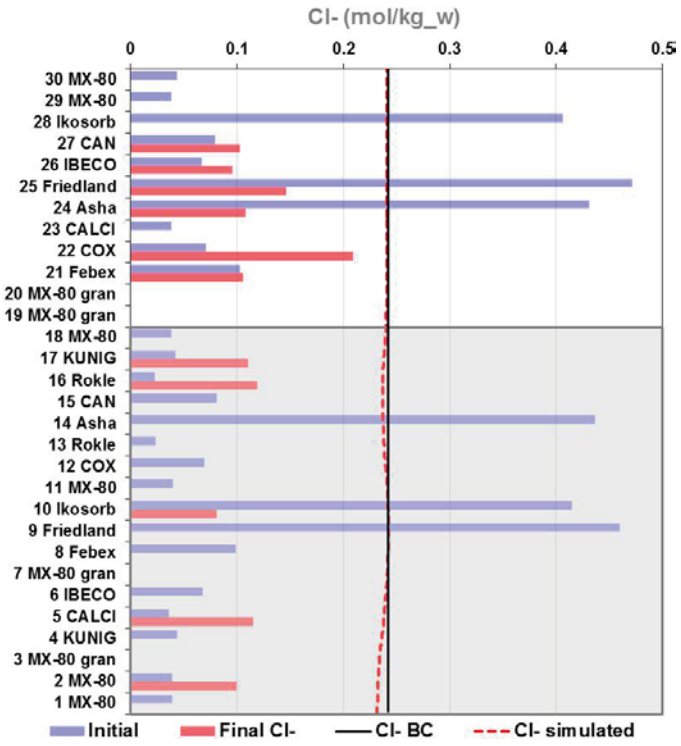

Figure 3-4. *Experimental (bars) and simulated (red dashed line) chloride concentration in ABM Package 1: before the test (blue bars) and after dismantling at 880 days (red bars). The boundary chloride concentration is also shown (black line). The shadowed blocks 1 to 18 represent the closed (no-flux) boundary condition in the simulation (see Figure 3-2 left).*

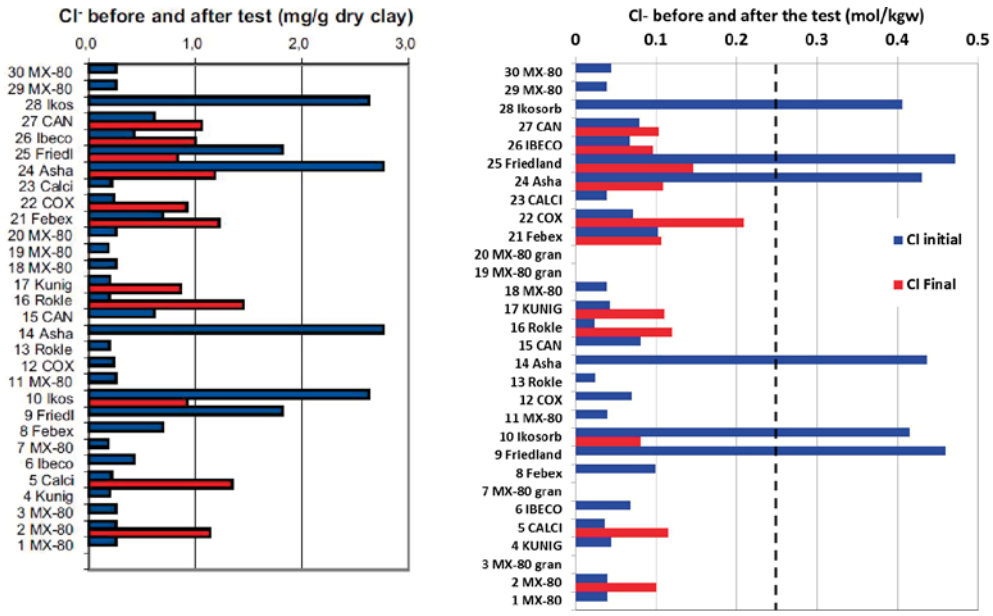

Figure 3-5. *Chloride concentrations in individual blocks of Package 1 before (blue) and after (red) the field test (Svensson et al. 2011): in mg/g dry clay (left), and in mol/kg of water (right). The values are calculated as the average concentration of the 3 or 5 samples analysed from each block (see Figure 3-6). The right plot also indicates the groundwater chloride concentration (dashed line).*

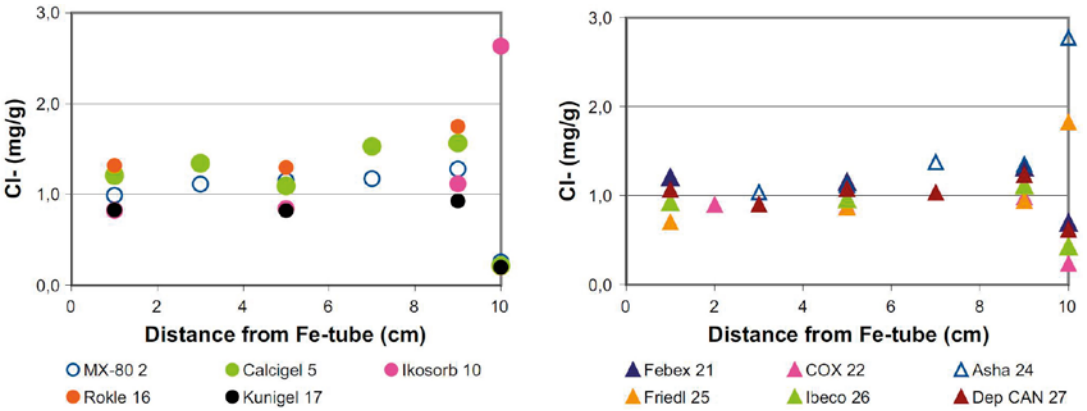

Figure 3-6. *Radial distribution of Cl^- (mg/g dry clay) in water extracts of the bentonite from the lower (left) and upper (right) part of the ABM package 1. The reference samples are plotted at the position 10 cm. Type of bentonite and block position in the package indicated in the legend (Svensson et al. 2011).*

Table 3-1. Groundwater composition: borehole KA2598A (Svensson et al. 2011).

Species	Concentrations	
pH	**7.33**	
Unit	**mg/L**	**mol/kg$_w$**
Na	2470	0.10744
K	12.4	0.00032
Ca	2560	0.06387
Mg	64.8	0.00267
HCO_3	51.7	0.00085
Cl	8580	0.24201
SO_4	483	0.00536
SO4_S	171	0.00190
Br	59	0.00074
F	1.5	0.00008
Si	6.3	0.00022

It is remarkable that the chloride concentration of the groundwater used for saturation (0.242 mol/kgw) differs significantly from the chloride concentrations measured in Package 1 blocks after the test (average value of 0.118 mol/kgw), except for the block made of Callox (0.209 mol/kgw), while it is stated that 'almost constant' concentrations (in radial direction) have been reached (Svensson et al. 2011). The horizontal profiles do not show a clear trend of persisting concentration gradients, meaning that horizontal diffusion has indeed almost stopped. Therefore, there must be some additional process that is responsible for this difference in concentrations at equilibrium.

3.1.3 Modelling of chloride exclusion in the ABM field test

To investigate this behaviour further, a set of scoping calculations have been performed to test different models and hypotheses:

1. Chloride dilution by mixing with groundwater during water saturation.
2. Donnan equilibrium model (Birgersson and Karnland 2009).
3. Multi-porosity model.

Given that the results from the ABM field test show a rather homogenized chloride concentration across the package thickness as well as across the different blocks, little information can be deduced about the transient diffusion of anions during the test. Therefore, it has been decided here to limit the analysis of anion exclusion to steady state conditions, i.e. after equilibrium has been reached. This approximation has the advantage that it allows to focus on the effect of the different microstructural models for compacted bentonite on chloride exclusion, neglecting the transient treatment of the diffusion process. In this way, the analysis is greatly simplified and a larger number of models can be tested.

Chloride dilution by mixing with groundwater during water saturation

First, we considered the case where groundwater enters the clay by advection with no anion exclusion during saturation and assuming that osmotic effects or Donnan equilibrium do not hold in this system. Then, chloride concentrations of the saturated blocks can be calculated by simple mixing as follows:

$$Cl^-_{sat} = S_{e_{ini}} \cdot Cl^-_{ini} + \left(1 - S_{e_{ini}}\right) \cdot Cl^-_{gw} \qquad \text{(Equation 3-1)}$$

where Cl^-_{sat} (mol/kgw) is the bentonite chloride concentration under water saturated conditions, $S_{e_{ini}}$ (-) is the initial degree of saturation of a given block, Cl^-_{ini} (mol/kgw) is its initial chloride concentration, and Cl^-_{gw} (mol/kgw) is the groundwater chloride concentration at the package boundary. This leads to the comparison with the experimental measurements shown in Figure 3-7.

It may be observed that the water saturation process following the hypotheses described above leads, in many of the blocks analysed, to similar chloride concentrations to those measured after the test (blocks 2 MX-80, 5 CALCIGEL, 16 Rokle, 17 Kunigel, 21 Febex, 22 COX, 26 IBECO, 27, Deponit CAN). By contrast, the three blocks with the highest initial chloride concentrations that have been analysed after the test (10 Ikosorb, 24 Asha, and 25 Friedland, see Figure 3-5) still show important differences. In these blocks the final concentrations measured are much smaller than those calculated using Equation 3-1. This analysis indicates that the water saturation process is not the only responsible for the homogenization of chloride concentrations. Moreover, in these calculations the potential anion exclusion effect during saturation and chloride diffusion in the bentonite are totally neglected.

Single-porosity Donnan equilibrium model

Another possible way to explain the low chloride concentrations in the blocks with respect to the boundary concentration in the ABM test is to use the concept of Donnan equilibrium (see Section 2.2.5). Considering Donnan equilibrium between the boundary groundwater concentration and the single porosity (i.e. the montmorillonite interlayer space) bentonite blocks, one could calculate the chloride concentration of the blocks in equilibrium with an external solution (Birgersson and Karnland 2009). Note that equilibrium implies that diffusion and advection have reached steady state conditions. It also implies that the equilibrium concentration in each block does not depend on the initial chloride concentration of the given block, but on the concentration at the boundary. This assumption is thought to be approximate enough for the purpose of comparing this equilibrium state with the experimental observations which are close to equilibrium. To calculate this equilibrium, the system of equations 2.24 and 2.27 needs to be solved (Leroy et al. 2007, Appelo and Wersin 2007, Birgersson and Karnland 2009).

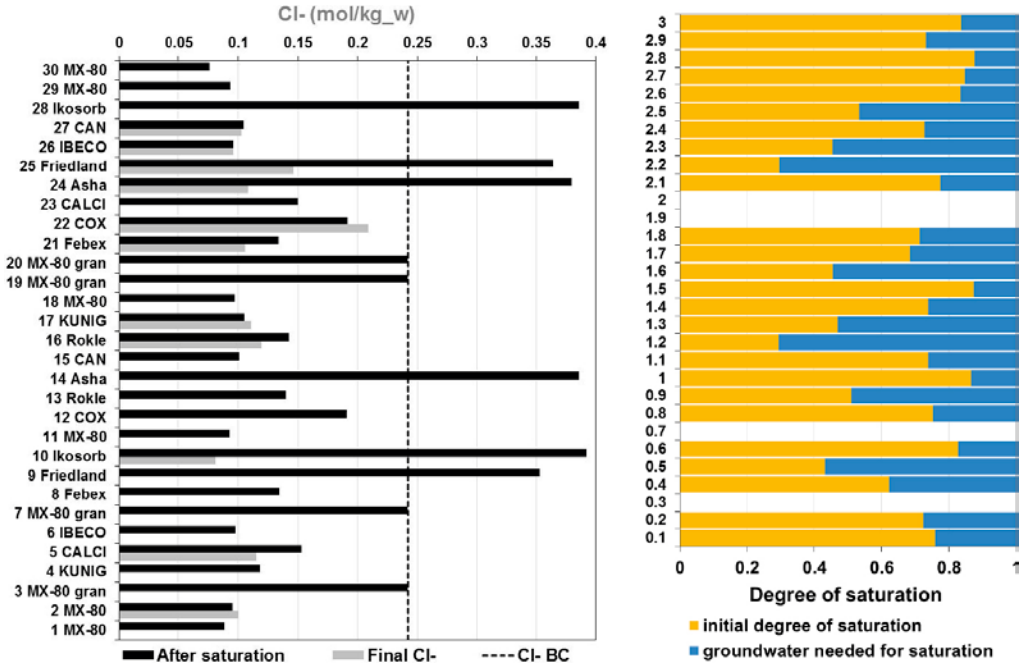

Figure 3-7. *Chloride concentrations in mol/kgw (left): experimental measurements after the test (grey), calculated concentrations after complete water saturation assuming conservative mixing – Equation 3-1 (black), and groundwater concentration at the boundary (dashed line). Initial degree of water saturation of the different blocks (right).*

For the system Ca-Na-Mg-K-Cl-SO4, which is representative of the ABM test environment, these equations can be reformatted, plugging Equation 2-24 in Equation 2-27, as follows:

$$-2\cdot\frac{a_{SO_4^{2-}}^{ext}}{\gamma_{SO_4^{2-}}^{int}}\cdot\Xi^4-\frac{a_{Cl^-}^{ext}}{\gamma_{Cl^-}^{int}}\cdot\Xi^3-c_{IL}\cdot\Xi^2+\left(\frac{a_{Na^+}^{ext}}{\gamma_{Na^+}^{int}}+\frac{a_{K^+}^{ext}}{\gamma_{K^+}^{int}}\right)\cdot\Xi+2\cdot\left(\frac{a_{Ca^{2+}}^{ext}}{\gamma_{Ca^{2+}}^{int}}+\frac{a_{Mg^{2+}}^{ext}}{\gamma_{Mg^{2+}}^{int}}\right)=0 \qquad \text{(Eq. 3-2)}$$

The internal concentrations can then be calculated from:

$$c_{Cl^-}^{int}=\Xi\cdot\frac{a_{Cl^-}^{ext}}{\gamma_{Cl^-}^{int}} \qquad \text{(Equation 3-3)}$$

$$c_{SO_4^{2-}}^{int}=\Xi^2\cdot\frac{a_{SO_4^{2-}}^{ext}}{\gamma_{SO_4^{2-}}^{int}} \qquad \text{(Equation 3-4)}$$

$$c_{Na^+}^{int}=\Xi^{-1}\cdot\frac{a_{Na^+}^{ext}}{\gamma_{Na^+}^{int}} \qquad \text{(Equation 3-5)}$$

$$c_{Ca^{2+}}^{int}=\Xi^{-2}\cdot\frac{a_{Ca^{2+}}^{ext}}{\gamma_{Ca^{2+}}^{int}} \qquad \text{(Equation 3-6)}$$

$$c_{K^+}^{int}=\Xi^{-1}\cdot\frac{a_{K^+}^{ext}}{\gamma_{K^+}^{int}} \qquad \text{(Equation 3-7)}$$

$$c_{Mg^{2+}}^{int}=\Xi^{-2}\cdot\frac{a_{Mg^{2+}}^{ext}}{\gamma_{Mg^{2+}}^{int}} \qquad \text{(Equation 3-8)}$$

The quartic function in Equation 3-2 needs to be solved for Ξ, the ion equilibrium coefficient. Subsequently, the internal ionic concentrations can be calculated from Equations 3-3 to 3-8.

The data required to solve these equations was calculated using PhreeqC and the thermodynamic database SIT.dat (Specific ion Interaction Theory), which is suitable for a wide range of ionic strength of the solution (from 0 up to 6 M). The calculated activities of the ions in the external solution are shown in Table 3-2. These calculations were performed at 25 °C. Different activity coefficients would be obtained at ~100 °C (see discussion of high temperature effects below): the same PhreeqC calculation at 100 °C yields lower activity coefficients (6 % lower for monovalent ions Na, K, and Cl, and 22 % lower for bivalent ions Ca, Mg, and SO_4).

Note that in order to solve Equation 3-5, the activity coefficients of the ions in the internal solution are also needed, which are not known a priori. However, here it is assumed that in the single porosity model under study the concentration of cations in the pore water solution equals the CEC. In this way, the ionic strength of the pore water may be estimated. Assuming typical CEC and final water content values of the field experiment (average values of 0.72 eq/kg dry clay and 0.29, respectively) and a calcium occupancy of around 60 % (approximate value after the test in the upper part of the package), the calculated ionic strength is ~3. Note that this treatment contrasts with the calculations by other scientists (Leroy et al. 2007, Jougnot et al. 2009), who stated that for CallOx argillite the activity coefficients in the pore solution are similar to those in the reservoir in contact with the porous medium.

This high ionic strength requires the use of SIT activity correction or other suitable approach such as Pitzer. In this work, SIT database has been used. The activity coefficients γ for the different ions in the internal solution are shown in Table 3-3. A comparison of the SIT correction method with the more classical extended Debye Hückel (eDH) approach (valid for low ionic strength solutions, up to 0.1 M) is also given in the table.

Table 3-2. Groundwater composition: molalities and activities of the ions involved in this study as calculated with PhreeqC. Temperature of the solution is 25 °C.

External water (I~0.3 M) using SIT database		
Species*	**Activity coefficient**	**Activity (M)**
Na^+	0.711	0.07419
K^+	0.701	0.000216
Ca^{2+}	0.261	0.01564
Mg^{2+}	0.268	0.0006102
Cl^-	0.721	0.1722
SO_4^{2-}	0.234	0.0008141

* Not totals.

Table 3-3. Pore water activity coefficients of the ions included in this study as calculated with PhreeqC and the databases SIT.dat (SIT approach) and phreeqc.dat (eDH). Temperature of the solution is 25 °C.

Activity corrections for pore water with I~3 M			
	***γ* SIT**	***γ* eDH***	**Ratio SIT/eDH**
Na^+	0.697	0.849	0.82
K^+	0.575	0.564	1.02
Ca^{2+}	0.111	0.333	0.33
Mg^{2+}	0.112	0.471	0.24
Cl^-	0.753	0.564	1.34
SO_4^{2-}	0.105	0.100	1.05

* eDH stands for extended Debye Huckel.

Using the data in Tables 3-2 and 3-3[1]. The results of the equilibrated internal chloride concentrations are compared with the experimental observations in Figure 3-8. The average chloride concentration assuming Donnan equilibrium is 0.0868 mol/kgw, which is ~26 % smaller than the average value of 0.118 mol/kgw of the experimental results (after the test).

[1] The quartic function was solved for each block (http://www.1728.org/quartic.htm)

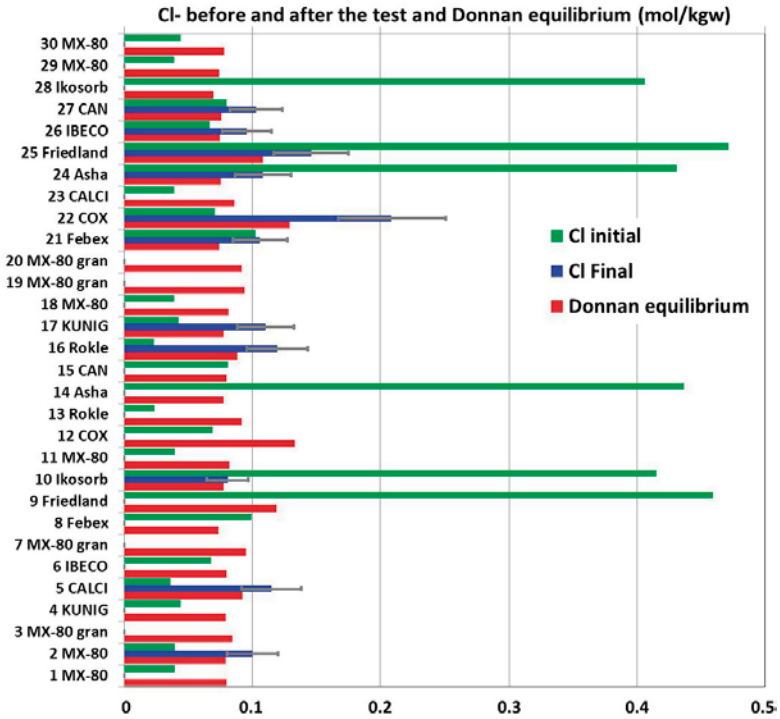

Figure 3-8. *Chloride concentrations in mol/kgw: experimental measurements before (green) and after (blue) the test, and calculated concentrations assuming Donnan equilibrium and a temperature of 25 °C (red). Error bars in Cl^- final represent ±20 % relative difference (see discussion below).*

Note on the repeatability of chloride concentration measured experimentally

(Table 3-4): in Svensson et al. (2011), the reference samples (i.e. before the test) were measured by two laboratories at different times, yielding differences of between 6 and 18 % for the blocks with highest chloride concentrations. These differences increase up to between 65 and ~300 % for the blocks with lower chloride concentrations. For comparative purposes, Figure 3-8 includes error bars with an assumed value of ±20 % for the final chloride concentrations. It may be observed that the lower limits agree reasonably well with the Donnan equilibrium model, except for the Callovo Oxfordian clay (COX). However, COX composition contains only a small amount of smectite and large amounts of other minerals. For example, Gaucher et al. (2004) report a smectite volume fraction of 0.26, while quartz and calcite amount to 40 % of the total volume. For this type of microstructure the applicability of the Donnan equilibrium model is probably not valid, and multiple porosity models may be more appropriate in this case.

Table 3-4. Measured chloride concentrations (ppm) from 2 laboratories of the reference samples. Data gathered from Svensson et al. (2011). LAB 1 at Äspo HRL; LAB 2 at ClayTech (only ClayTech analysed the final chloride concentrations).

	LAB 1 Cl^-	LAB 2 Cl^-	Difference
Material	(mg/kg dry clay)		(L1-L2)/L1
Asha505	2988	2770	7.30 %
Calcigel	64	210	−228.13 %
Callovo-Oxfordian	76	230	−202.63 %
DeponitCAN	744	610	18.01 %
Febex	652	690	−5.83 %
Friedland	1939	1820	6.14 %
IbecoSeal	255	430	−68.63 %
Ikosorb	3106	2630	15.33 %
Kunigel	51	200	−292.16 %
MX80	156	260	−66.67 %
Rokle	48	190	−295.83 %

High temperature effects

The previous results have been obtained assuming a temperature of 25 °C for the geochemical calculations of activity coefficients. During the thermal period (i.e. during the field test), the equilibrium between external and internal concentrations depends on the ion equilibrium coefficient (Donnan) that is a function of temperature, see Equation 2-24, and therefore is prone to changes when cooling. However, in the ABM test cooling occurs at the time of (or shortly after) dismantling and thus the establishment of this new equilibrium is hindered because the system is closed (meaning that the interaction with external groundwater is not possible anymore).

Equation 3-2 is solved for Ξ using input data based on activities of the geochemical system. The dependence of activity coefficients on temperature may therefore significantly affect the results of Equation 3-2. To account for this effect, activities and activity coefficients of the external groundwater and internal porewater species have been recalculated with PhreeqC at 100 °C, using otherwise the same database and setup. The results are shown in Table 3-5. Important differences are found, especially for the bivalent ions Ca, Mg and SO_4 , and to a less extent for the monovalent ones (Na, K, and Cl).

Table 3-5. Calculated activities (M) and activity coefficients of different ions for the solutions presented in Table 3-2 (I = 0.3 M) and Table 3-3 (I = 0.3 M): effect of temperature.

Species	Activity coefficient, γ		Activity (M)	
I = 0.3 M	25 °C	100 °C	25 °C	100 °C
Na	0.711	0.668	7.42E−02	6.97E−02
K	0.701	0.659	2.16E−04	2.01E−04
Ca	0.261	0.203	1.56E−02	1.21E−02
Mg	0.268	0.209	6.10E−04	4.93E−04
Cl	0.721	0.678	1.72E−01	1.61E−01
SO_4	0.234	0.183	8.14E−04	7.03E−04
I = 3 M	**25 °C**	**100 °C**		
Na	0.697	0.631		
K	0.575	0.521		
Ca	0.111	0.075		
Mg	0.112	0.076		
Cl	0.753	0.684		
SO_4	0.105	0.071		

These values have been used to recalculate the quartic function. It has also been assumed that the final CEC values have decreased by an average of 10 % with respect to the initial values as measured on the reference samples (see Dohrmann et al. 2013 for a discussion on CEC values). The results of the equilibrated internal chloride concentrations are compared with the experimental observations in Figure 3-9. The comparison with experimental results at 100 °C is remarkably good for all the blocks. The average chloride concentration is now 0.100 mol/kgw, 15 % lower than the measured average value. This comparison indicates that Donnan equilibrium is a plausible explanation of the different concentrations between the package porewater and the external groundwater. It also captures the significant decrease of chloride concentrations in the blocks with initially high contents (blocks 10, 24, and 25).

The calculated ion equilibrium coefficient for the different blocks ranges between 0.34 (blocks with highest CEC) and 0.64 (blocks with lowest CEC). From these coefficients, the mean electrical potential can be calculated using Equation 2-24, yielding values between −14.9 and −36.3 mV (with a mean value of −29.4 mV). For comparison, the mean electrical potential of the entire pore space of the COX clay-rock was determined to be in the range −15 to −40 mV (Jougnot et al. 2009).

This approach also enables the calculation of the occupancy of the cation exchanger of the different blocks. Using Equations 3-5 to 3-8, the cationic concentrations can be calculated, from which the occupancy of the cation exchanger can been derived for each block. The average occupancies for Ca^{+2}, Na^{+}, Mg^{+2}, and K^{+} are shown in Table 3-6. It is observed that the Donnan model largely overestimates

the calcium increase of the exchanger at the expense of sodium, with little variation between different blocks. Interestingly, magnesium is underestimated, as in the previous model (Pękala et al. 2012). Therefore, the Donnan equilibrium model is not fully consistent in the sense that only chloride concentrations are successfully estimated, while important differences are still observed in the cation exchanger composition.

Table 3-6. Cation exchanger composition: experimentally measured vs. Donnan equilibrium model values.

	Calculated exchanger composition (unity fraction)			
Model	**Na^{+}**	**Ca^{+2}**	**K^{+}**	**Mg^{+2}**
Average	12.27 %	84.26 %	0.04 %	3.42 %
Minimum	10.15 %	79.20 %	0.04 %	3.22 %
Maximum	17.52 %	86.30 %	0.06 %	3.51 %
Experimental*	**Na^{+}**	**Ca^{+2}**	**K^{+}**	**Mg^{+2}**
Average	28.40 %	58.00 %	2.30 %	11.50 %
Minimum	19.00 %	41.00 %	1.00 %	7.00 %
Maximum	49.00 %	65.00 %	5.00 %	16.10 %

* Experimental values correspond to the upper part of the package (blocks 21 to 30), for which it is thought that equilibrium with groundwater has been almost reached.

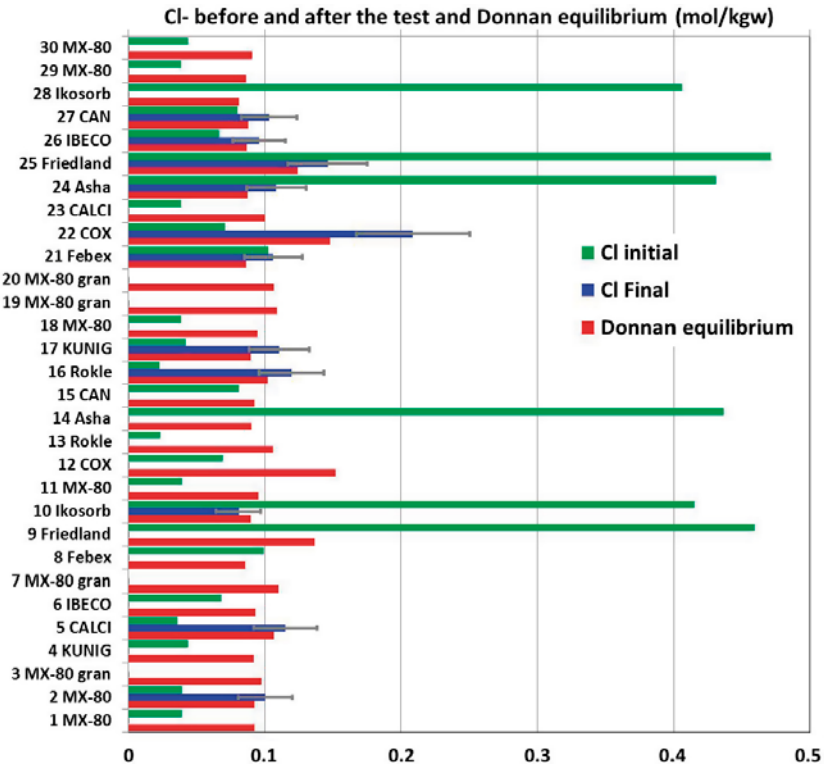

Figure 3-9. *Chloride concentrations in mol/kgw: experimental measurements before (green) and after (blue) the test, and calculated concentrations assuming Donnan equilibrium and a temperature of 100 °C (red). Error bars in* Cl^{-} *final are assumed to be ±20 % (see discussion above).*

Multi-porosity model

Alternative explanations for the discrepancy between measured groundwater and porewater chloride concentrations could involve anion accessible porosity and how it affects chloride concentrations from per mass of material into per mass (or litre) of pore water. The measured chloride contents are reported per mass of (dry) bentonite. In order to recalculate this to per litre of pore water (and assuming complete water saturation of the pore space), the value of porosity must be known. In the present study this recalculation (see Figure 3-5) was carried out utilising the total (physical) porosity (ϕ_{tot}), which was calculated according to the standard Equation 2-1. The dry and grain densities needed to calculate porosities are reported in Svensson et al. (2011) for the ABM field test. For example, porosities calculated for MX-80 bentonite blocks using the final dry densities are in the range 0.44–0.48.

However, if the porosity value used was not representative of the "effective" or "accessible" chloride porosity, this would lead to an error in the calculated chloride concentration as per pore water volume: for a chloride accessible porosity smaller than the total, using the total porosity value would result in a recalculation error to the effect of lowering the calculated concentration (due to an artificial "dilution effect"). Given the above premise, it is investigated below whether such a dilution effect could account quantitatively for the above-mentioned discrepancy between chloride concentrations measured (and recalculated to mol/L of pore water) in the bentonite and the boundary groundwater value.

First, the effect of anion exclusion due to electrostatic restriction of chloride concentrations in the DDL has been studied for MX-80 bentonite. Figure 3-10 shows a continuous chloride profile concentration (solid black line) along the pore thickness as a function of distance from the charged montmorillonite surface, located at zero distance (Modified Gouy-Chapman model from Tournassat and Appelo 2011). A specific (total) surface area of montmorillonite of 749 m^2/g (e.g. Bradbury and Baeyens 2002) and a CEC of 0.81 mol_c/kg were assumed to calculate surface charge with NaCl concentration of 0.1 mol/L. It can be seen from the figure that the distance over which chloride concentrations are (visibly) affected by the electric potential associated with the surface charge is on the order of 3–4 nm.

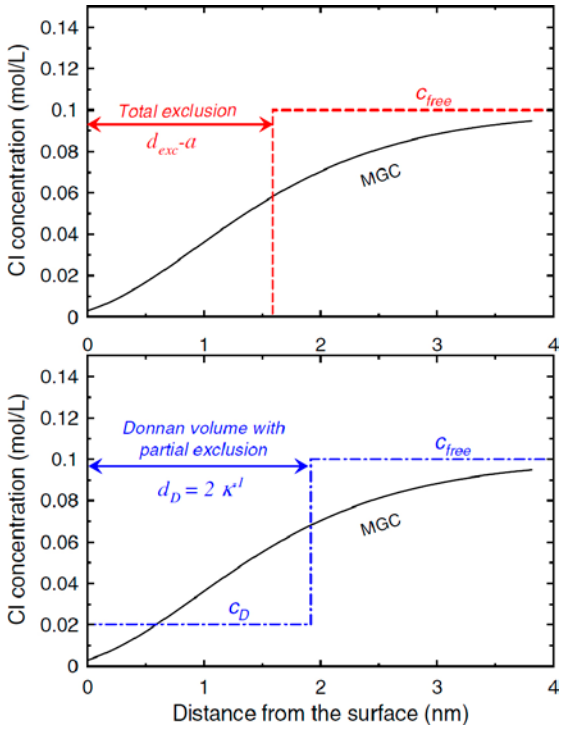

Figure 3-10. *Chloride concentration in the EDL (mol/L) as a function of distance away from the charged surface (nm) according to (i) MGC model (black curve), (ii) total anion exclusion distance (dashed red line on top figure), and (iii) Donnan approximation with a Donnan volume extending up to two Debye lengths from the surface position (blue line on bottom figure). From Tournassat and Appelo (2011).*

The extent of Donnan thickness can be calculated according to Equation 2-8. The values calculated for a Debye length number (λ) equal to two and three for the conditions of the ABM experiment (external chloride concentration of 0.24 M) are 1.225 nm and 1.8375 nm, respectively. It can be observed from the figure that the extent of the Donnan volume corresponding to total exclusion distance (~ 1.55 nm, red line in Figure 3-10) falls in the calculated range using Equation 2-8 and assuming λ = 2 and λ = 3. Therefore, it seems reasonable to assume a Debye length number λ = 2 for the following calculations of DDL porosity. As a limiting case of maximum dilution, complete anion exclusion from the DDL space was assumed in the considerations that follow.

Calculations presented below are based on the following general methodology and assumptions:

- Three types of porosity are considered to be present: interlayer (IL), diffuse layer (DDL) and free.
- The IL porosity is calculated based on geometric considerations of the montmorillonite structure (crystal cell dimensions, cell stacking and internal surface area of montmorillonite), and complete anion exclusion from this porosity is assumed.
- The DDL porosity is calculated from the DDL length (a function of ionic strength and the Debye length number, which is assumed to be equal to two) and using montmorillonite's external surface area). Anions are assumed to be completely excluded from the DDL porosity.
- The free water porosity is calculated from the difference between the total porosity (Equation 3-12) and the sum of IL and DDL porosities. Anions can only be present in the free porosity.

Additional details on the methodology utilised are presented in Section 2.1. The calculations using Equations 2-1 to 2-6 were carried out with the parameters shown in Table 3-7 and Table 3-8. The dry density for each block was assumed equal to the final values (i.e. measured after the experiment) from Svensson et al. (2011) – see Table 3-8 (which also shows the values of montmorillonite content used).

The DDL thickness (t_{DDL}) was estimated from Equation 2-8, where κ^{-1} was calculated using an ionic strength of 0.24 M. The DDL porosity was calculated according to Equation 2-7. The values of montmorillonite content in the different blocks used in the calculations are presented in Table 3-8. As a first approximation, values of external surface area for all blocks were assumed to be equal to the MX-80 value (45 m^2/g; Karnland 2010).

Table 3-7. Constant and parameter values used for the calculation of the interlayer porosity.

Parameter	Symbol	Value	Unit
[1]Montmorillonite crystal unit-cell dimension	a	5.23×10^{-10}	m
[1]Montmorillonite crystal unit-cell dimension	b	9.05×10^{-10}	m
[1*]Montmorillonite crystal unit-cell dimension	c*	9.60×10^{-10}	m
[1]Stacking number in the ***a*** direction	n_a	200	–
[1]Stacking number in the ***b*** direction	n_b	200	–
[2,†]Stacking number in the ***c*** direction	n_c	5	–
Molecular weight	M_w	0.735	kg/mol
[3]Total Cl concentration in free water	m_{ext}	0.24	mol/L
[1]Solution density ration interlayer/free water	f_{dens}	1	–
Montmorillonite crystal density	ρ_s	2760	kg/m^3

c* is the orthogonally projected c-axis.

[†]base case value.

[1]Appelo (2013).

[2]Pusch (2001).

[3]Svensson et al. (2011).

Table 3-8. Bentonite dry density (Svensson et al. 2011) and montmorillonite content used in calculations.

Bentonite/clay type	Bentonite dry density [kg/m^3]	Montmor. Content [%]
MX80	1463	75
Kunigel V1	1661	47
Calcigel	1427	70
Ibeco Seal	1428	81
Febex	1438	80
Friedland	1817	30
Ikosorb	1456	70
Callovo Oxfordian	1982	26
Rokle	1408	72
Asha 505	1481	70
Deponit CAN	1463	81

The results of the calculations are presented in Table 3-9. It can be seen from the table that for most of the blocks the concentrations modelled according to the methodology presented above, and assuming complete chloride exclusion from the IL and DDL space, are in fair agreement with the values measured (and recalculated).

Table 3-9. Summary of results. Porosities are refered to 1L of medium (porosities related with Equation 2-2). Modelled chloride values assume complete anion exclusion from IL and DDL porosities. Measured values recalculated from per mass of dry bentonite to per volume of pore water. Relative difference [%] expressed with respect to the measured values (absolute). Cl_{mod} – Cl modelled, Cl_{exp} – Cl measured from experiment.

Bentonite Block	Total porosity [-]	Volume IL [L]	Volume DDL [L]	Volume FREE [L]	Cl modelled [mol/L]	Cl measured [mol/L]	Relative % difference 1-Cl_{mod}/Cl_{exp}
MX80	0.470	0.236	0.062	0.172	0.088	0.100	12
Kunigel V1	0.380	0.203	0.044	0.133	0.084	0.111	24
Calcigel	0.470	0.242	0.057	0.171	0.087	0.115	24
Ibeco Seal	0.480	0.242	0.066	0.172	0.086	0.096	10
Febex	0.470	0.240	0.065	0.165	0.084	0.106	21
Friedland	0.360	0.177	0.031	0.152	0.101	0.146	31
Ikosorb	0.470	0.237	0.058	0.175	0.089	0.081	−10
Callovo Oxfordian	0.260	0.149	0.029	0.081	0.075	0.209	64
Rokle	0.500	0.245	0.058	0.197	0.095	0.119	21
Asha 505	0.520	0.233	0.059	0.228	0.105	0.108	3
Deponit CAN	0.470	0.236	0.067	0.167	0.085	0.103	17

It is seen from the table that the modelled chloride concentrations are close to the measured values, except for the Callovo Oxfordian claystone, where the modelled value is substantially lower (by 64 %) than the measured one. It is noted that in all cases, the model values are lower than the corresponding measured concentrations (except for Ikosorb). This is in part due to the assumption of total anion exclusion from the DDL and IL porosities. Partial anion exclusion from these porosities (at least for the DDL) would therefore lead to a closer comparison. Therefore, this structural model can quantitatively explain the observed discepancy between chloride concentrations recalculated from measured data (~0.1 M) and concentrations predicted by equilibration with the boundary groundwater (0.24 M).

As a result, it may be interpreted that chloride concentrations in the bentonite blocks are likely close to the values measured in the boundary groundwater, but restricted to an anion accessible porosity only (anion exclusion). Hence, when measured chloride values (per mass) are recalculated into molarity (per volume of pore water), these calculations should only consider a fraction of the total porosity, which is accessible to chloride. According to the model, chloride is likely to be strongly excluded from the DDL and IL porosities. However, it can also be seen that the modelled chloride values are consistently below the measured and recalculated ones. Although the difference is small, this could indicate that chloride exclusion from these porosities is not complete, but partial, as suggested by the Donnan equilibirum assumption.

The sensitivity of the model for bentonite MX-80 was studied considering three key parameters: vertical stacking of montmorillonite platelets (n_c), montmorillonite content in the bentonite, and bentonite density. The results for combined effects of vertical stacking (varied between 2 and 25) and two values of montmorillonite content (70 % and 90 %) are shown in Figure 3-11. It is seen from the figure that within the expected values (3 to 7, see Pusch 2001) the vertical stacking number can change the modelled concentrations by about 30 %, while a 20 % change in montmorillonite content results in less than 15 % difference.

The sensitivity of the model to the value of bentonite dry density is shown in Figure 3-12. The calculation was carried out for two values of bentonite dry density, i.e. 1559 and 1435 kg/m^3. These are the most divergent, final (i.e. after the experiment) values measured for all MX-80 bentonite blocks (Svensson et al. 2011). It is seen from Figure 3-12 that, within the expected values of the vertical stacking number (3 to 7, see Pusch 2001), variation of bentonite dry density between 1435 and 1559 kg/m^3 results in less than 25 % relative difference of the calculated chloride concentrations.

3.2 Modelling diffusion in compacted bentonite

This section presents a quantitative inter-comparison of a selection of approaches that have been recently used to model solute diffusion through compacted bentonite by other researchers. These methodologies were applied to calculate steady state diffusive flux (blind prediction) of trace concentrations of NaCl considering the following conceptual set-up (Figure 3-13):

- The bentonite is MX-80, where its physical and chemical properties are defined based on the ABM test (Svensson et al. 2011)
- Bentonite is 0.35 m long (distance for diffusion), which is the expected radial dimension of the buffer in the KBS-3V concept
- Physical (total) porosity of the bentonite is calculated as a function of the dry density using Equation 2-1
- Bentonite is fully saturated with aqueous solution of 0.24 M NaCl (background electrolyte)
- At the inlet end of the bentonite column a constant concentration of tracer NaCl (Na-tracer and Cl-tracer) of 10^{-6} M is applied, while at the exit end a constant zero concentration is maintained (note that no background NaCl diffusion is considered)
- Tracer diffusion through bentonite is assumed to have reached steady state

The goal of this exercise is to investigate the quantitative impact of using various approaches to calculating solute diffusion in bentonite, and to assess the relative benefits and disadvantages of those approaches. Table 3-10 lists the approaches considered in the exercise.

For Approach 1 the methodology previously described in Section 2.1 (Appelo 2013) was used. Input data for the calculation is shown in Table 3-11.

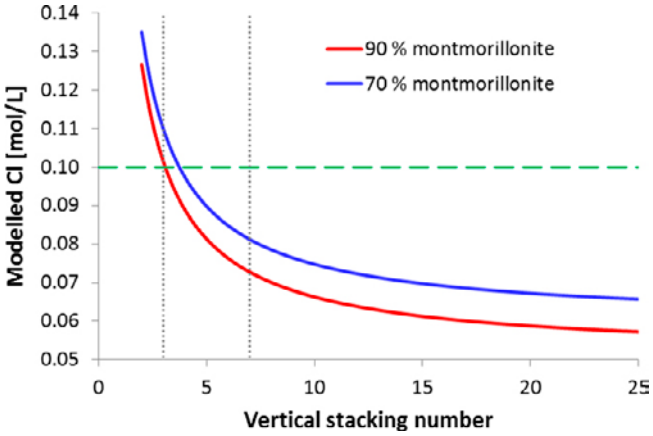

Figure 3-11. *Chloride concentrations calculated for MX-80 bentonite assuming complete chloride exclusion from the IL and DDL porosities as a function of vertical stacking and for two values of montmorillonite content (90 % and 70 %). Horizontal dashed line indicate the measured and recalculated chloride concentration (0.1 M). Vertical dotted lines indicate expected vertical stacking values (n_c = 3 to 7 – Pusch 2001 and Melkior et al. 2009, as cited by Tournassat and Appelo 2011).*

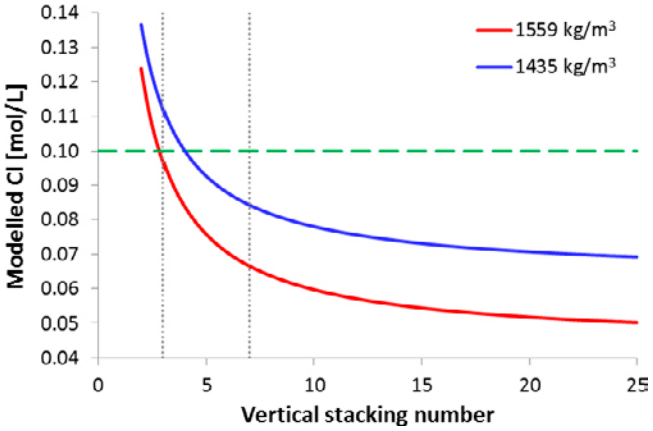

Figure 3-12. *Chloride concentrations calculated for MX-80 bentonite assuming complete chloride exclusion from the IL and DDL porosities as a function of vertical stacking and for two values of dry bentonite density (1559 and 1435 kg/m^3). The horizontal dashed lines indicates the measured and recalculated chloride concentration (0.1 M). The two vertical dotted lines indicate expected vertical stacking values (3 and 7 – Pusch 2001 and Melkior et al. 2009, as cited by Tournassat and Appelo 2011).*

Table 3-10. Approaches considered for modelling of NaCl tracer duffusion in MX-80 compacted bentonite.

Approach numerical identifier	Description	Reference
1	Multi-porosity (free, DDL and IL)	Appelo (2013)
2	Semi-empirical	Van Loon et al. (2007)
3	Single porosity, Donnan equilibrium	Birgersson and Karnland (2009)
4	Empirical	Ochs and Talerico (2004)
5	Empirical	Wersin et al. (2014)

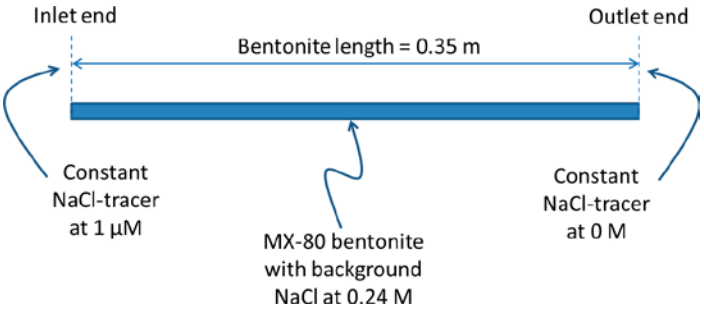

Figure 3-13. *Conceptual set-up for comparative modelling of NaCl tracer diffusion through MX-80 bentonite.*

Table 3-11. Input data used for Approach 1 calculations.

Parameter	Value
Total porosity[1]	0.47
CEC (per solid mass)[2]	0.79 (eq/kg)
External surface area[3]	45 (m^2/g)
Internal surface area[4]	749 (m^2/g)
CEC (per total water)	1.156[†] (eq/L)
CEC (per IL water)	4.621[†] (eq/L)
CEC (per DDL water)	1.052[†] (eq/L)
Surface charge (per DDL water)	−1.052[†] (eq/L)

[†]Base case value calculated for bentonite dry density of 1463 (kg/m^3).
[1]Calculated from Equation 2-1.
[2]Bradbury and Baeyens (2003).
[3]Karnland (2010).
[4]Bradbury and Baeyens (2002).

Three cases, using different values of bentonite dry density, were considered for Approach 1 calculations:

- Base case: bentonite dry density of 1463 kg/m^3 (dry density of MX-80 measured after the ABM experiment; Svensson et al. 2011).
- Low bentonite density of 1300 kg/m^3 (lower limit for sensitivity calculations).
- High bentonite density of 1600 kg/m^3 (upper limit for sensitivity calculations).

The input and calculated tracer fluxes at steady state for the base case bentonite density of 1463 kg/m^3 are presented in Table 3-12.

Note that in Approach 1 calculations, the FREE, DDL and IL porosities (ϕ) were calculated using the multi-porosity approach of Appelo (2013; see Section 2.1). The tortuosity-constrictivity factors (δ/θ^2) were assumed identical for all three porosities and equal 0.1, while free water diffusion coefficients for Na^+ and Cl^- were taken from Appelo and Postma (2005). Moreover, chloride was assumed to be completely excluded from the IL space.

The fractional occupancy of the exchanger (β) for Na^+ tracer was estimated assuming isotopic equilibrium between the exchanger and the boundary water, hence the value 10^{-5}, which reflects the ratio of Na^+ tracer and Na^+ background in the boundary water. Similar assumption was made by Glaus et al. (2013), and it appears reasonable under steady state diffusion conditions.

Table 3-12. Input and calculated tracer fluxes at steady state for the Base Case bentonite density of 1463 kg/m³. NA – not applicable, NU – not used, ε – porosity, δ/θ² – tortuosity-constrictivity factor, D_w – free water diffusion coefficient, β – fractional occupancy of the exchanger (selectivity coefficient).

Compartment	ϕ	δ/θ²	0.1 M NaCl 1μM Cl^-	Gradient	D_w	Flux
FREE			**[mol/m³]**	**[mol/m⁴]**	**[m²/s]**	**[mol/m²/s]**
Cl^-	0.24	0.10	1.00E−03	2.86E−03	2.03E−09	1.41E−13
Na^+	0.24	0.10	1.00E−03	2.86E−03	1.33E−09	9.24E−14
DDL			**[mol/m³]**	**[mol/m⁴]**	**[m²/s]**	**[mol/m²/s]**
Cl^-	0.06	0.10	5.22E−04	NU	2.03E−09	1.68E−14
Na^+	0.06	0.10	1.10E−02	NU	1.33E−09	2.32E−13
IL			**β [-]**	**dβ/dx [1/m]**	**[m²/s]**	**[mol/m²/s]**
Cl^-	0.23	0.10	NA	NA	2.03E−09	NA
Na^+	0.23	0.10	1.00E−05	2.86E−05	1.33E−09	7.36E−13

Cl^- background concentration in the DDL was approximated using the following formula (Tournassat and Appelo 2011):

$$c_{D,Cl-} = \frac{2c_{free}^2}{-q + \sqrt{q^2 + 4c_{free}^2}} \qquad \text{(Equation 3-9)}$$

where c_{D,Cl^-} is the concentration of background Cl^- in the DDL, c_{free} is the concentration of background Cl^- in the free porosity, and q is the surface charge density as per litre of DDL pore water. The concentration of Cl^- tracer was then calculated from the ratio of tracer to background Cl^- ($=10^{-5}$).

Concentration of Na^+ background in the DDL was approximated from charge balance of the surface charge (equal to CEC per DDL water with opposite sign), and the concentration of Na^+ tracer was calculated from the ratio of tracer to background Na^+ ($=10^{-5}$).

The fluxes of NaCl tracer in the FREE, DDL and IL porosities were calculated following Appelo (2013) using Equations 3-10, 3-11 and 3-12, respectively:

$$J_{free,i} = -\phi_{free} \frac{\delta_{free}}{\theta_{free}^2} D_{w,i} \frac{dc_i}{dx} \qquad \text{(Equation 3-10)}$$

$$J_{DDL,i} = -\phi_{DDL} \frac{\delta_{DDL}}{\theta_{DDL}^2} D_{w,i} \frac{c_{DDL,i}}{c_i} \frac{dc_i}{dx} \qquad \text{(Equation 3-11)}$$

$$J_{IL,i} = -\phi_{IL} \frac{\delta_{IL}}{\theta_{IL}^2} D_{w,i} \left(\frac{c_{IL,CEC}}{|z_i|}\right) \frac{d\beta_i}{dx} \qquad \text{(Equation 3-12)}$$

where $J_{free,i}$, $J_{DDL,i}$ and $J_{IL,i}$ are the diffusive fluxes of species i in the free, DDL, and IL porosities, respectively, $\delta_{free}/\theta^2_{free}$, $\delta_{DDL}/\theta^2_{DDL}$, and $\delta_{IL}/\theta^2_{IL}$ are the constrictivity-tortuosity factors in free, DDL, and IL porosities, respectively, $D_{w,i}$ is the free water diffusion coefficient of species i, c_i and $c_{DDL,i}$ are the concentration of species i in free and DDL porosities, respectively, dc_i/dx is concentration gradient of species I (in the free porosity), $c_{IL,CEC}$ is the CEC concentration of species i in DDL, z_i is the charge of species i, and $d\beta_i/dx$ is concentration gradient of selectivity coefficient of species i.

A summary of the results from the calculations obtained following Approach 1 methodology are shown in Table 3-13 and graphically in Figure 3-14.

Approach 2 was used to calculate steady state flux of Cl^- using the semi-emipirical formulae of Van Loon et al. (2007) – Equations 2-31 and 2-32. The calculation considers background electrolyte concentration (ionic gstrength) of 0.24 M, and was carried out for two bentonite densities (for which relevant fitting parameter values were available): 1300 kg/m³ and 1600 kg/m³. Note that an average flux value (arithmetic mean) was calculated for bentonite density of 1450 kg/m³ assuming that

bentonite properies and fluxes scale linearly with density. Steady state fluxes were calculated by multiplying the concentration gradient of Cl^- tracer (10^{-3} mol/m^3 per 0.35 m = 2.86×10^{-3} mol/m^4) by the effective diffiusion coefficient estimated from Equations 2-32. Results of the calculation are shown in Table 3-13 and graphically in Figure 3-14.

Approach 3, based on the Donnan equilibrium assumption, was used to calculate the steady state flux of Cl^- tracer using Equations 2-28 and 2-29. The value of D_c (m^2/s), which is the model fitting parameter (equivalent to the pore diffusion coefficient for non-sorbing species), was estimated for different dry densities from the results in Brigersson and Karnland (2009): 1.80×10^{-10}, 1.49×10^{-10}, and 1.26×10^{-10} m^2/s for dry densities of 1300, 1463, and 1600, respectively. Total porosities (ϕ_c) are calculated using Equation 2-1 as a function of dry density. The ion equilibrium coefficient for each dry density (which affects the term *CEC/w* in Equation 2-26) was calculated using the methodology presented in Section 3.1.3, using the SIT database at a temperature of 25 °C, yielding values of 0.392, 0.349, and 0.314 for dry densities of 1300, 1463, and 1600, respectively. Thus, in this approach the effective diffusion coefficient is reduced by the ion equilibrium coefficient (which is equivalent to interprete it as a concentration drop at the bentonite-groundwater interface). The results of these calculations are shown in Table 3-13 and graphically in Figure 3-14.

Approach 4 calculates steady state flux of Cl^- tracer using the values of effective diffusion coefficient recommended by Ochs and Talerico (2004) – see Section 2.2.6. The calculation utilises the recommended value (10^{-11} m^2/s) as well as the upper (3×10^{-11} m^2/s) and lower (3×10^{-12} m^2/s) bounding values. These values were multiplied by the steady state Cl^- tracer gradient of 2.86×10^{-3} [mol/m^4] to calculate the "best guess", upper limit and lower limit flux, respectively. Results of this calculation are shown in Table 3-13 and graphically in Figure 3-14.

Approach 5 employs the empirical formula for effective diffusion coefficient of chloride in compacted bentonite derived by Wersin et al. (2014) – Equation 2-33. Using this approach, stead state flux of Cl^- tracer through bentonite of three different densities (1300 kg/m^3, 1460 kg/m^3 and 1600 kg/m^3) were calculated by multiplying the Cl^- tracer concentration gradient (2.86×10^{-3} mol/m^4) by the effective diffusion coefficient from Equation 2-33. Results of this calculation are shown in Table 3-13 and graphically in Figure 3-14.

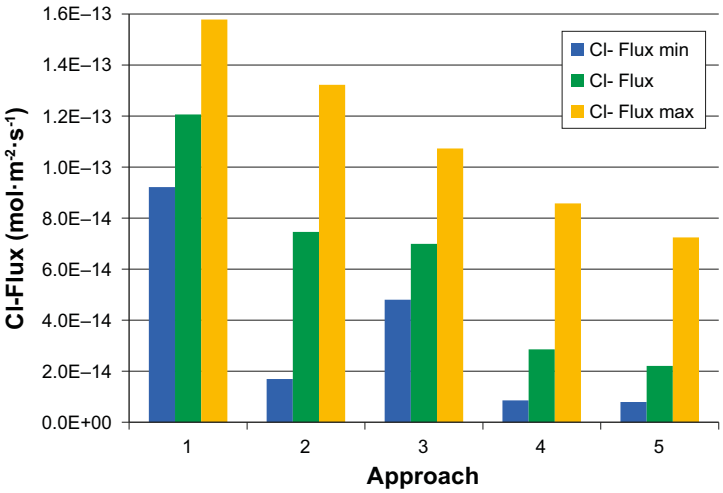

Figure 3-14. *Graphic representation of results shown in Table 3-13. Consult Table 3-10 for explanations on the approaches used.*

Table 3-13. A compilation of results on steady state diffusive flux of Cl^- tracer through the bentonite column calculated using the five different methodologies (approaches). Consult Table 3-10 for explanations on the approaches used.

Approach	Cl^- Flux min	Cl^- Flux	Cl^- Flux max
		mol/(m²·s)	
1†	9.21E−14	1.21E−13	1.58E−13
2††	1.69E−14	7.46E−14	1.32E−13
3†	4.80E−14	6.99E−14	1.07E−13
4†††	8.57E−15	2.86E−14	8.57E−14
5†	7.96E−15	2.20E−14	7.24E−14

† Cl^- flux min. (minimum) corresponds to bentonite density of 1300 kg/m³, flux corresponds to bentonite density of 1460 kg/m³, and flux max. (maximum) corresponds to bentonite density of 1600 kg/m³.

†† Cl^- flux min. (minimum) corresponds to bentonite density of 1300 kg/m³, Cl^- flux max. (maximum) corresponds to bentonite density of 1600 kg/m³. Cl^- flux is the average flux calculated as arithmetic mean of the minimum and maximum values.

††† Cl^- flux min., Cl^- flux and Cl^- flux max. correspond to the minimum, recommended and maximum values of effective diffusion coefficient for Cl^- (Ochs and Talerico 2004).

Table 3-13 and Figure 3-14 indicate that using the approaches described, the calculated "best guess" flux values are relatively similar (differ by less than a factor of six) with the multi-porosity approach (Approach 1) predicting the highest and the empirical formula of Wersin et al. (2014, Approach 5) predicting the lowest steady state Cl^- tracer flux. Interestingly, the flux calculated using the effective diffusion coefficient recommended by Ochs and Talerico (2004) for the SR-Can and SR-Site Performance Assessments is on the lower end of the scale. It should also be noted that the multi-porosity approach (Approach 1), while the most versatile, is at the same time the most complex of all approaches considered. This leads to a potentially significant uncertainty on the calculated values of flux. The high uncertainty reflects both limited conceptual understanding of the micro- and nano-structure of compacted bentonite as well as insufficient data on transport and electrochemical properties of the DDL and IL (such as tortuosity and water permittivity in the different porosities – Leroy et al. 2006, Appelo 2013). On the other hand, the simplified approaches could be considered more reliable at present, but at the price of being less flexible in handling complex or changing conditions.

It may be of interest to compare the fluxes calculated specifically for Cl^- tracer with a prediction based on the transport of an uncharged species (e.g. HTO – tritiated water). The formulae provided by Ochs and Talerico (2004), Equation 3-13, and Wersin et al. (2014), Equation 3-14, are the following:

$$D_e = 6.7785 \times 10^{-9} \times e^{-2.5671 \times 10^{-3} \times \rho_d} \quad \text{(Equation 3-13)}$$

$$D_e = 3.0 \times 10^{-9} \times e^{-2.2 \times 10^{-3} \times \rho_d} \quad \text{(Equation 3-14)}$$

The effective diffusion coefficient of HTO can be estimated as a function of bentonite dry density (ρ_d). A calculation performed for three dry bentonite densities of 1300 kg/m³, 1460 kg/m³ and 1600 kg/m³ using Equation 3-13 gives Cl^- tracer fluxes of 6.88×10^{-13}, 4.53×10^{-13} and 3.19×10^{-13} mol/(m² · s), respectively. These values are significantly higher (on average by a factor of ~10) than those calculated with Approaches 1-5 (Table 3-13), which take account of anion exclusion (smaller accessible porosity and higher tortuosity).

Diffusive fluxes were also calculated for a cation, namely Na^+ tracer, using Approaches 1 (multi-porosity), 3 (Donnan equilibrium), 4, and 5. Approach 2 is only applicable for anions and has therefore not been used for Na^+. Ochs and Talerico (2004, Approach 4) and Wersin et al. (2014, Approach 5) both propose to estimate the diffusion coefficient of non-sorbing cations with the same formula used for HTO (Equations 3-13 and 3-14, respectively). Therefore, these expressions can also be used to calculate the fluxes of Na^+ tracer.

The calculated fluxes are shown in Table 3-14. The reason why the Donnan equilibrium model has also been used with a dry density of 1950 kg/m^3 for Na^+ tracer is because the value of D_c for Na^+ (2.9×10^{-11} m^2/s) has been fitted from a Na^+ tracer experiment (Glaus et al. 2007) at such a high dry density. For lower dry densities, the values of D_c are those published for Cl^- (Birgersson and Karnland 2009, Figure 10).

Table 3-14. Steady state fluxes of Na^+ tracer through the bentonite column calculated with Approach 1 (multi-porosity) for three different values of bentonite dry density.

	Bentonite dry density			
Approach	1300 kg/m^3	1460 kg/m^3	1600 kg/m^3	1950 kg/m^3
	Steady state flux (mol·m^{-2}·s^{-1})			
1	4.01E−12	4.47E−12	4.86E−12	–
2*	–	–	–	–
3	5.54E−12	5.13E−12	4.75E−12	1.31E−12
4	6.88E−13	4.53E−13	3.19E−13	
5	4.91E−13	3.43E−13	2.54E−13	

* Not applicable.

Compared to the values calculated for anions (and the uncharged HTO, using Approaches 4 and 5), Na^+ tracer fluxes are roughly an order of magnitude higher using approaches 1 and 3. Unexpectedly, the calculated flux using Approach 1 increases slightly with bentonite dry density, which is contrary to experimental observations. On the other hand, the fluxes calculated using Approaches 3, 4 and 5 show a decrease with increasing dry density. To understand the reason of this unexpected result, Figure 3-15 shows the calculated porosities and Na^+ tracer fluxes separately for the individual pore spaces using Approach 1.

It can be seen that with increasing bentonite density the free porosity drops (calculated using Equation 2-2 from the total porosity derived from Equation 2-1 and therefore a function of dry density). However, Na^+ transport is strongly dominated by the IL, at least for the parameterization described above, whose porosity remains more or less independent of density in this range (Figure 2-3, right). At the same time, the CEC (mol/$L_{interlayer}$) increases proportionally with dry density (Figure 3-16).

Consequently, the gradient term in Equation 3-12 increases, and so does the flux. Given that this behaviour contradicts experimental results and conceptual expectation, it possibly indicates that an important assumption has been misused. A likely candidate here could be related with the tortuosity-constrictivity factor of the IL, which was assumed to be the same for all three porosities (equal 0.1).

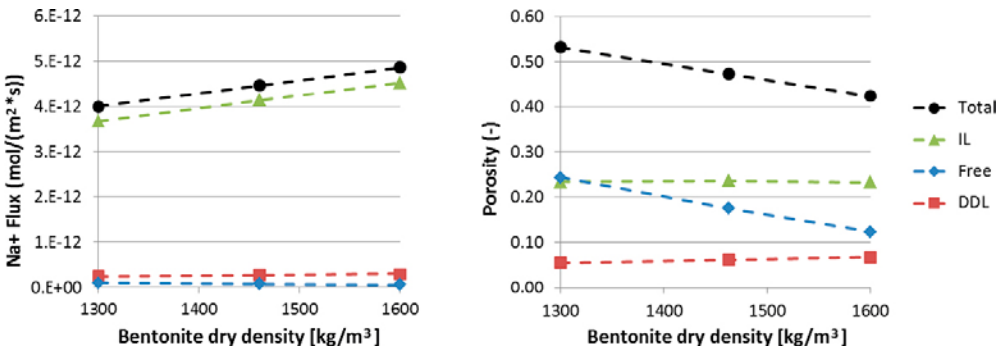

Figure 3-15. *Porosities and Na^+ tracer flux in the distinct pore spaces calculated for bentonite dry densities of 1300 kg/m^3, 1460 kg/m^3 and 1600 kg/m^3. IL – interlayer, DDL – diffuse double layer, Free – free (bulk) solution, and Total is the physical porosity (sum of IL, DDL and Free).*

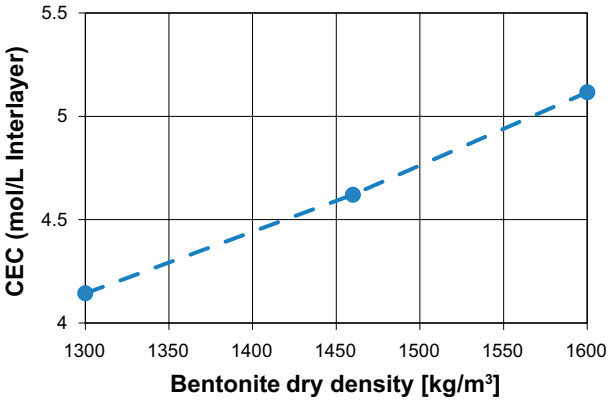

Figure 3-16. *Interlayer CEC expressed as per liter of interlayer water, as a function of bentonite dry density.*

It is likely that the value of this parameter varies between the porosities, and also (for a given porosity) with changing bentonite dry density. For example, Bourg and Sposito (2010) demonstrated from molecular dynamics calculations that the diffusion coefficient in the IL varies with the degree of hydration of Na in the interlayer (which correlates with bentonite swelling and hence with bentonite dry density). This variation is quite considerable, e.g. the diffusion coefficient in the IL changes by about 50 % with the transition from 3-layer to 2-layer hydrates in the IL, which would have the effect of reducing Na^+ diffusion in the IL by this same factor (~50 %).

3.3 A short note on the LOT A2 experiment

The models presented in previous sections have also been used to assess the anion concentrations in a similar field experiment, namely the LOT A2 field experiment at Äspö HRL (Karnland et al. 2009). In this case, the bentonite column is made entirely of MX-80 bentonite blocks so that the experimental results are more homogeneous than the ABM field test.

First, using the same mixing model of saturation with groundwater and applying Equation 3-1, chloride concentrations in the case of MX-80 bentonite have been calculated. It is found that the agreement is remarkably good (differences smaller than 2 %), see Table 3-10. This assumption has also been successfully used for the same experiment in Sena et al. (2010a).

Table 3-10. Comparison of chloride concentrations using Equation 3-1 and experimentally measured for the LOT A2 experiment.

Variable	Data in Sena et al. (2010a)	
Se_{ini}	0.5	–
$Cl^-_{Aspo\ groundwater}$	0.1780	mol/L
$Cl^-_{ini\_MX80}$	0.0400	mol/L
$Cl^-_{after\ saturation}$ (using Eq. 3.1)	0.1090	mol/L
Experimental: average block 1	0.1072	mol/L
Experimental: average block 2	0.1086	mol/L

The Donnan equilibrium model has also been applied in this case, using similar assumptions regarding activities calculations (SIT database, 100 °C). The groundwater (external) and MX-80 bentonite porewater activities (internal) are shown in Table 3-11, together with the results. The comparison in this case is not as good as in the ABM case: the Donnan model predicts an equilibrated concentration of 0.0642 mol/kgw, i.e. 40 % lower than the average value of 0.1072 mol/kgw measured experimentally.

In turn, the results using the multi-porosity model are presented in Table 3-12. Similarly to the Donnan equilibrium model, the modelled concentrations are lower (by 46 %) than the measured values. Therefore, for this particular field test, it would seem as if the mixing with groundwater during saturation is a more relevant process.

Table 3-11. Donnan equilibrium model applied to LOT A2 experiment: input and output data.

Solution	External (I ~ 0.25 M)		Internal (I ~ 2.8 M)	
Species	**Activity (M)**	**γ**	**Activity (M)**	**γ**
Ca	1.14E−02	0.2178	2.83E−02	0.0738
Cl	1.21E−01	0.6902	5.15E−02	0.6699
K	1.70E−04	0.6730	1.50E−02	0.5176
Mg	3.22E−04	0.2223	8.99E−03	0.0745
Na	6.39E−02	0.6808	7.50E−01	0.6471
S	6.71E−04	0.2009	2.70E−03	0.0522
Average water content (-)			0.3	
Average CEC (eq/kg dry clay)			0.82	
Ion equilibrium coefficient			0.355	
Cl^- internal (mol/kgw)			0.0642	

Table 3-12. Results of the multi-porosity model applied to LOT A2 experiment. Porosities are refered to 1L of medium (porosities related with Equation 2-2). Modelled chloride values assume complete anion exclusion from IL and DDL porosities. Relative difference [%] expressed with respect to the measured values (absolute). Cl_{mod} – Cl modelled, Cl_{exp} – Cl measured from experiment.

Bentonite	Total porosity [-]	Volume IL [L]	Volume DDL [L]	Volume FREE [L]	Cl modelled [mol/L]	Cl measured [mol/L]	Relative % difference $1\text{-}Cl_{mod}/Cl_{exp}$
MX80 (LOT-A2)	0.460	0.236	0.074	0.151	0.058	0.108	46

4 Discussion and conclusions

A literature review of different diffusion models in compacted bentonite has been conducted. The discrepancy between different conceptualizations of the bentonite pore structure is identified as the main obstacle towards a well-accepted theory for ionic transport in this type of materials.

A general formulation for a multi-component and multi-porosity diffusion model has been presented, which is based on what has been implemented in the geochemical codes PhreeqC and Crunchflow. It considers the Nernst-Planck equations for electrochemical diffusion, three types of porosity (free, double layer, and interlayer), diffusion in each porosity type following its own tortuosity, and coupled to cation exchange and surface complexation reactions. From this general formulation, it is then possible to obtain more simplified models by simply changing the parameterization, thus providing flexibility to the user.

A special case is the model by Birgersson and Karnland (2009), with a single porosity governed exclusively by Donnan equilibrium. This case cannot be implemented in current geochemical codes due to the fact that the formulation in these codes relies upon the composition of the solution in the free porosity (it assumes that some free porosity always exists). Therefore, a non-zero free porosity needs to be present, although it may be substantially reduced. The minimum free porosity value will in general be limited by numerical convergence constraints.

In the present study, two sets of scoping calculations have been performed in order to evaluate different microstructural and diffusion models for compacted bentonite. In the first set, the experimental data from the ABM field test (Svensson et al. 2011), in which near-equilibrium conditions were reached, has been used to test different microstructural models at equilibrium. In this case, no diffusion coefficients or fluxes need to be calculated. Instead, measured anion (chloride) concentrations in the ABM package 1 are used to elucidate which microstructural model can better explain the experimental observations. The results show that the single-porosity Donnan equilibrium model (Birgersson and Karnland 2009) is, after correcting for temperature and electrostatic effects, able to predict the chloride concentrations measured experimentally after the field test (although cation occupancy in the exchanger is not well captured). A multi-porosity model with total anion exclusion from the interlayer and the diffuse double layer also explains the chloride results qualitatively, with differences below 25 % for most of the blocks. On the other hand, a simple chloride dilution model by mixing with groundwater during saturation cannot satisfactorily explain the observed results.

As a summary of the first set of scoping calculations, it may be stated that:

- A Fick's diffusion single porosity model (using any effective diffusion coefficient) coupled to cation exchange reactions is able to capture the behaviour of the cation exchange occupancy of the ABM field test (Pękala et al. 2012), but fails to explain the diffusion of anions.
- The Donnan equilibrium model is able to explain measured chloride concentrations in the ABM field test, but fails to explain the cation exchange occupancies.
- The multi-porosity model is also able to explain measured chloride concentrations in the ABM field test. In principle, cation exchange occupancies (not modelled here) can be included with standard cation exchange reactions (as done in Pękala et al. 2012) coupled to the multi-porosity model. Since the cation exchange reactions would be calculated in equilibrium with the free pore water composition, and since the latter is almost in equilibrium with the boundary groundwater composition (i.e. similar concentrations), it is expected that the cation exchange occupancy would be similar to the results obtained in Pękala et al. (2012). Therefore, this approach, if coupled with cation exchange reactions, seems to be the most consistent model to explain the ABM experimental observations.

As an additional test, the Donnan equilibrium, the multi-porosity, and the simple mixing models have also been used to assess the concentration of chloride measured on another field test on MX-80 bentonite, namely the LOT-A2 test (Karnland et al. 2009). In this case, the Donnan equilibrium and the multi-porosity models fail to explain the chloride concentrations, while a remarkable agreement

is found between measured values and the simple mixing model by saturation with groundwater. Therefore, the conclusions presented above need to be taken with caution.

In the second set of scoping calculations, different mechanistic and empirical or semi-empirical models were used to calculate the steady state flux of Cl^- and Na^+ tracers through compacted bentonite with a thickness representative of the buffer in the KBS-3V repository concept, and assuming boundary conditions that maximize the diffusive flow (namely a zero concentration is imposed at the outflow boundary, equivalent to assume a fast flush out by surrounding groundwater flow). This methodology enables the comparison of different diffusion models by simple calculations at steady state. The results indicate that the fluxes are comparable between the different models (best guesses differ by less than a factor of six), which is a consequence of the similarity between the different effective diffusion coefficients, except for chloride diffusion in the simple Fick's law formulation (as used e.g. in Sena et al. 2010b).

Independently of the diffusion model (and pore structure model) adopted, the parameterization is usually performed based on fitting of rather similar experimental data from through-diffusion experiments using measured diffusion fluxes, effective or apparent diffusion coefficients, concentration profiles, and/or accessible porosity for anions. Therefore, it is not surprising that the final values of fluxes at steady state for the through-diffusion setup studied do not differ significantly between the models.

Combined, the results of both sets of scoping calculations suggest that even though the modelling of out-diffusion of radionuclides in the event of canister failure could be represented by any of the studied models (second set of simulations), the concentrations of species within the bentonite can differ significantly between the different models (first set of simulations). In addition, the lack of consensus on the conceptualization of compacted bentonite microstructure has implications for providing a complete and mechanistic understanding of the system. This is specially the case when comparing different conceptualizations of bentonite considered in the modelling of different physic-chemical processes, such as freezing, osmotic effects, and swelling. Ideally, future research efforts in each field (e.g. diffusion, swelling, or hydro-mechanical processes) should converge to the same microstructural conceptualization of compacted bentonite.

It is difficult to establish a priori whether one model is conservative (from a geochemical point of view) with respect to another or not, because it is not only the time at which a given solution composition is reached at the outflow or what is the steady state flux, but also the composition at the outlet itself (due to anion exclusion and electro-migration effects acting differently in each model).

Moreover, the multi-porosity models, despite their relative complexity and the related uncertainty, currently offer the only option to mechanistically account for complicated multi-physical coupling (such as might be expected under variable and coupled thermal-chemical-mechanical conditions). As such, these kinds of models are invaluable for the understanding of radionuclide diffusion through compacted bentonite buffer under the expected repository conditions.

References

SKB's (Svensk Kärnbränslehantering AB) publications can be found at www.skb.se/publications.

Appelo C A J, 2013. A review of porosity and diffusion in bentonite. Posiva Working Report 2013-29, Posiva Oy, Finland.

Appelo C A J, Postma D, 2005. Geochemistry, groundwater and pollution. 2nd ed. Leiden: Balkema.

Appelo C A J, Wersin P, 2007. Multicomponent diffusion modeling in clay systems with application to the diffusion of tritium, iodide, and sodium in Opalinus Clay. Environmental Science & Technology 41, 5002–5007.

Appelo C A J, Van Loon L R, Wersin P, 2010. Multicomponent diffusion of a suite of tracers (HTO, Cl, Br, I, Na, Sr, Cs) in a single sample of Opalinus Clay. Geochimica et Cosmochimica Acta 74, 1201–1219.

Apted M, Arthur R, 2012. Initial review of chemical and erosional processes within the buffer and backfill – Geochemical processes. Technical Note 2012-29, Strålsäkerhetsmyndigheten /(Swedish Radiation Safety Authority).

Arthur R, 2010. Handling of hydrogeochemical relations in erosion and swelling pressure models for the buffer and backfill. STUK-TR 10, Radiation and Nuclear Safety Authority, Finland.

Bazer-Bachi F, Tevissen E, Descostes M, Grenut B, Meier P, Simonnot M-O, Sardin M, 2005. Characterization of iodide retention on Callovo-Oxfordian argillites and its influence on iodide migration. Physics and Chemistry of the Earth, Parts A/B/C 31, 517–522.

Birgersson M, Karnland O, 2009. Ion equilibrium between montmorillonite interlayer space and an external solution – Consequences for diffusional transport. Geochimica et Cosmochimica Acta 73, 1908–1923.

Boudreau B P, Meysman F J R, Middelburg J J, 2004. Multicomponent ionic diffusion in porewaters: Coulombic effects revisited. Earth and Planetary Science Letters 222, 653–666.

Bourg I C, Sposito G, 2010. Connecting the molecular scale to the continuum scale for diffusion processes in smectite-rich porous media. Environmental Science & Technology 44, 2085–2091.

Bourg I C, Bourg A C M, Sposito G, 2003. Modeling diffusion and adsorption in compacted bentonite: a critical review. Journal of Contaminant Hydrology 61, 293–302.

Bourg I C, Sposito G, Bourg A C M, 2007. Modeling cation diffusion in compacted water-saturated sodium bentonite at low ionic strength. Environmental Science & Technology 41, 8118–8122.

Bradbury M H, Baeyens B, 2002. Porewater chemistry in compacted re-saturated MX-80 bentonite: physico-chemical characterisation and geochemical modeling. PSI Bericht Nr. 02-10, Paul Scherrer Institut, Switzerland.

Bradbury M H, Baeyens B, 2003. Porewater chemistry in compacted re-saturated MX-80 bentonite. Journal of Contaminant Hydrology 61, 329–338.

Cavé L, Al T, Xiang Y, Loomer D, 2010. Investigations of diffusive transport processes in sedimentary rock. NWMO TR-2010-04, Nuclear Waste Management Organization, Canada.

Dohrmann, R, Olsson S, Kaufhold S, Sellin P, 2013. Mineralogical investigations of the first package of the alternative buffer material test II. Exchangeable cation population rearrangement. Clay Minerals 48, 215–233.

Dzombak D A, Morel F M M, 1990. Surface complexation modeling: hydrous ferric oxide. New York: Wiley.

Eriksen T E, Jansson M, Molera M, 1999. Sorption effects on cation diffusion in compacted bentonite. Engineering Geology 54, 231–236.

Gaucher E, Robelin C, Matray J M, Négrel G, Gros Y, Heitz J F, Vinsot A, Rebours H, Cassagnabère A, Bouchet A, 2004. ANDRA underground research laboratory: interpretation of the mineralogical and geochemical data acquired in the Callovian-Oxfordian formation by investigative drilling. Physics and Chemistry of the Earth, Parts A/B/C 29, 55–77.

Gimmi T, Kosakowski G, 2011. How mobile are sorbed cations in clays and clay rocks? Environmental Science & Technology 45, 1443–1449.

Glaus M A, Baeyens B, Bradbury M H, Jakob A, Van Loon L R, Yaroshchuk A, 2007. Diffusion of ^{22}Na and ^{85}Sr in montmorillonite: evidence of interlayer diffusion being the dominant pathway at high compaction. Environmental Science & Technology 41, 478–485.

Glaus M A, Birgersson M, Karnland O, Van Loon L R, 2013. Seeming steady-state uphill diffusion of $^{22}Na^{+}$ in compacted montmorillonite. Environmental Science & Technology 47, 11522–11527.

Hedström M, Karnland O, 2012. Donnan equilibrium in Na-montmorillonite from a molecular dynamics perspective. Geochimica et Cosmochimica Acta 77, 266–274.

Holmboe M, Wold S, Jonsson M, 2012. Porosity investigation of compacted bentonite using XRD profile modeling. Journal of Contaminant Hydrology 128, 19–32.

Jougnot D, Revil A, Leroy P, 2009. Diffusion of ionic tracers in the Callovo-Oxfordian clay-rock using the Donnan equilibrium model and the formation factor. Geochimica et Cosmochimica Acta 73, 2712–2726.

Karnland O, 2010. Chemical and mineralogical characterization of the bentonite buffer for the acceptance control procedure in a KBS-3 repository. SKB TR-10-60, Svensk Kärnbränslehantering AB.

Karnland O, Olsson S, Dueck A, Birgersson M, Nilsson U, Hernan-Håkansson T, Pedersen K, Nilsson S, Eriksen T E, Rosborg B, 2009. Long term test of buffer material at the Äspö Hard Rock Laboratory, LOT project. Final report on the A2 test parcel. SKB TR-09-29, Svensk Kärnbränslehantering AB.

Kato H, Muroi M, Yamada N, Ishida H, Sato H, 1995. Estimation of effective diffusivity in compacted bentonite. In Murakami T, Ewing R C (eds). Scientific basis for nuclear waste management XVIII: symposium held in Kyoto, Japan, 23–27 October 1994. Pittsburgh, PA: Materials Research Society. (Materials Research Society Symposium Proceedings 353), 277–284.

Kozaki T, Sato H, Fujishima A, Saito N, Sato S, Ohashi H, 1997. Effect of dry density on activation energy for diffusion of strontium in compacted sodium montmorillonite. In Gray W J, Triay I R (eds). Scientific basis for nuclear waste management XX: symposium held in Boston, Massachusetts, USA, 2–6 December 1996. Pittsburgh, PA: Materials Research Society. (Materials Research Society Symposium Proceedings 465), 893–900.

Kozaki T, Liu J, Sato S, 2008. Diffusion mechanism of sodium ions in compacted montmorillonite under different NaCl concentration. Physics and Chemistry of the Earth, Parts A/B/C 33, 957–961.

Kozaki T, Sawaguchi T, Fujishima A, Sato S, 2010. Effect of exchangeable cations on apparent diffusion of Ca^{2+} ions in Na- and Ca-montmorillonite mixtures. Physics and Chemistry of the Earth, Parts A/B/C 35, 254–258.

Krabbenhøft K, Krabbenhøft J, 2008. Application of the Poisson–Nernst–Planck equations to the migration test. Cement and Concrete Research, 38, 77–88.

Kraepiel A M L, Keller K, Morel F M M, 1999. A model for metal adsorption on montmorillonite. Journal of Colloid and Interface Science 210, 43–54.

Leroy P, Revil A, Coelho D, 2006. Diffusion of ionic species in bentonite. Journal of Colloid and Interface Science 296, 248–255.

Leroy P, Revil A, Altmann S, Tournassat C, 2007. Modeling the composition of the pore water in a clay-rock geological formation (Callovo-Oxfordian, France). Geochimica et Cosmochimica Acta 71, 1087–1097.

Mayer K U, Amos R T, Molins S, Gérard F, 2012. Reactive transport modeling in variably saturated media with MIN3P: basic model formulation and model enhancements. In Zhang F, Yeh G-T, Parker J C (eds). Groundwater reactive transport models. Oak Park, IL: Bentham Science Publishers, 186–211.

Molera M, Eriksen T, Jansson M, 2003. Anion diffusion pathways in bentonite clay compacted to different dry densities. Applied Clay Science 23, 69–76.

Muurinen A, Rantanen J, Penttilä-Hiltunen P, 1985. Diffusion mechanisms of strontium, cesium and cobalt in compacted sodium bentonite. In Werme L O (ed). Scientific basis for nuclear waste management IX: symposium held in Stockholm, Sweden, 9–11 September 1985. Pittsburgh, PA: Materials Research Society. (Materials Research Society Symposium Proceedings 50), 617–624.

Muurinen A, Karnland O, Lehikoinen J, 2004. Ion concentration caused by an external solution into the porewater of compacted bentonite. Physics and Chemistry of the Earth, Parts A/B/C 29, 119–127.

Muurinen A, Karnland O, Lehikoinen J, 2007. Effect of homogenization on the microstructure and exclusion of chloride in compacted bentonite. Physics and Chemistry of the Earth, Parts A/B/C 32, 485–490.

Ochs M, Talerico C, 2004. SR-Can. Data and uncertainty assessment. Migration parameters for the bentonite buffer in the KBS-3 concept. SKB TR-04-18, Svensk Kärnbränslehantering AB.

Ochs M, Lothenbach B, Wanner H, Sato H, Yui M, 2001. An integrated sorption–diffusion model for the calculation of consistent distribution and diffusion coefficients in compacted bentonite. Journal of Contaminant Hydrology 47, 283–296.

Oscarsson D W, 1994. Surface diffusion: is it an important transport mechanism in compacted clays? Clays and Clay Minerals 42, 534–543.

Parkhurst D L, Appelo C A J, 2013. Description of input and examples for PHREEQC version 3 – a computer program for speciation, batch-reaction, one-dimensional transport, and inverse geochemical calculations. U.S. Geological Survey.

Pękala M, Idiart A, Arcos D, 2012. Reactive transport modeling of the ABM experiment with Comsol Multiphysics. In Clays in natural and engineered barriers for radioactive waste confinement: International meeting on clays in natural and engineered barriers for radioactive waste confinement, Montpellier France, 22–25 October 2012, 905–906.

Ponte Castañeda P, Suquet P, 1998. Nonlinear composites. Advances in Applied Mechanics 34, 171–302.

Pusch R, 2001. The microstructure of MX-80 clay with respect to its bulk physical properties under different environmental conditions. SKB TR-01-08, Svensk Kärnbränslehantering AB.

Samson E, Marchand J, Robert J-L, Bournazel J-P, 1999. Modelling ion diffusion mechanisms in porous media. International Journal for Numerical Methods in Engineering 46 2043–2060.

Sato H, Ashida T, Kohara Y, Yui M, Sasaki M, 1992. Effect of dry density on diffusion of some radionuclides in compacted sodium bentonite. Journal of Nuclear Science and Technology 29, 873–882.

Sato H, Yui M, Yoshikawa H, 1995. Diffusion behavior for Se and Zr in sodium-bentonite. In Murakami T, Ewing R C (eds). Scientific basis for nuclear waste management XVIII: symposium held in Kyoto, Japan, 23–27 October 1994. Pittsburgh, PA: Materials Research Society. (Materials Research Society Symposium Proceedings 353), 269–276.

Savage D, 2012. Prospects for coupled modelling. STUK-TR 13, Radiation and Nuclear Safety Authority, Finland.

Sena C, Salas J, Arcos D, 2010a. Thermo-hydro-geochemical modelling of the bentonite buffer. LOT-A2 experiment. SKB TR-10-65, Svensk Kärnbränslehantering AB.

Sena C, Salas J, Arcos D, 2010b. Aspects of geochemical evolution of the SKB near field in the frame of SR-Site. SKB TR-10-59, Svensk Kärnbränslehantering AB.

SKB, 2010. Data report for the safety assessment SR-Site. SKB TR-10-52, Svensk Kärnbränslehantering AB.

Snyder K A, Marchand J, 2001. Effect of speciation on the apparent diffusion coefficient in nonreactive porous systems. Cement and Concrete Research 31, 1837–1845.

Steefel C, 2008. Crunchflow. Multicomponent reactive flow and transport software. User's manual. Lawrence Berkeley National Laboratory. Available at http://www.csteefel.com/CrunchFlowIntroduction.html

Steefel C, Rutqvist J, Tsang C F, Liu H H, Sonnenthal E, Houseworth J, Birkholzer J, 2010. Reactive transport and coupled THM processes in engineering barrier systems (EBS), LBNL-3901E, Lawrence Berkeley National Laboratory.

Svensson D, Dueck A, Nilsson U, Olsson S, Sandén T, Lydmark S, Jägerwall S, Pedersen K, Hansen S, 2011. Alternative buffer material. Status of the ongoing laboratory investigation of reference materials and test package 1. SKB TR-11-06, Svensk Kärnbränslehantering AB.

Tachi Y, Yotsuji K, 2014. Diffusion and sorption of Cs^+, Na^+, I^- and HTO in compacted sodium montmorillonite as a function of porewater salinity: integrated sorption and diffusion model. Geochimica et Cosmochimica Acta 132, 75–93.

Tournassat C, Appelo C A J, 2011. Modelling approaches for anion-exclusion in compacted Na-bentonite. Geochimica et Cosmochimica Acta 75, 3698–3710.

Van Loon L R, Glaus M A, Müller W, 2007. Anion exclusion effects in compacted bentonites: Towards a better understanding of anion diffusion. Applied Geochemistry 22, 2536–2552.

Wersin P, 2003. Geochemical modelling of bentonite porewater in high-level waste repositories. Journal of Contaminant Hydrology 61, 405– 422.

Wersin P, Curti E, Appelo C A J, 2004. Modelling bentonite–water interactions at high solid/liquid ratios: swelling and diffuse double layer effects. Applied Clay Science 26, 249–257.

Wersin P, Kiczka M, Rosch D, 2014. Safety case for the disposal of spent nuclear fuel at Olkiluoto. Radionuclide solubility limits and migration parameters for the canister and buffer. Posiva 2012-39, Posiva Oy, Finland.

Appendix A

Performance of diffusion models

The cpu time needed to solve a given setup using the Nernst-Planck equations as a function of the amount of species transported has been assessed. Results of a simple 3D model of the Nernst-Planck and Fick's law equations using Comsol are presented, where the dependence of the simulation time on the number of species, their charge, and the approach (Fick's law or Nernst-Planck equations) has been studied in detail.

The 3D mesh of the column is presented in Figure A-1. The results are presented in terms of cpu time as a function of the number of transported species in Figure A-2. As expected, it is observed that the case of Fick's diffusion leads to much smaller cpu times than the Nernst-Planck equations. Moreover, in the case of the Nernst-Planck equations, the cpu time depends almost linearly on the number of species. In addition, the cpu time of the solution of the Nernst-Planck equations depends substantially on the charge of the species (note the different slope of the curves). In the case where all species are neutral, the simulation time is reduced by a factor of 2.5–3.0 with respect to the case of all charged species. This reduction is due to the fact that for neutral species, the migration term in Equation 2-1 vanishes (it depends on z_i), thus simplifying the solution of the equation.

This is observed more clearly in Figure A-3, which compares the simulation times for two cases of 50 and 100 species with different charges and also using Fick's law. A case with a mix of charged and neutral species is also presented, which falls in between the cases of all neutral and all charged species. This mix is more representative of a real situation, in which neutral secondary species are also found. For instance, in the system Al-C-Ca-Cl-Fe-K-Na-S-Si-Sr using the Thermochimie thermodynamic database[2] from a total of 165 species (master and secondary species), ~35 % of them is neutral.

In conclusion, for a given number of species, the solution of the Nernst-Planck equations consumes significantly more cpu time than the Fick's law (more than one order of magnitude). In addition, the charge of the species transported determines to a large extent the cpu time needed, being the case of all neutral species the least cpu time consuming.

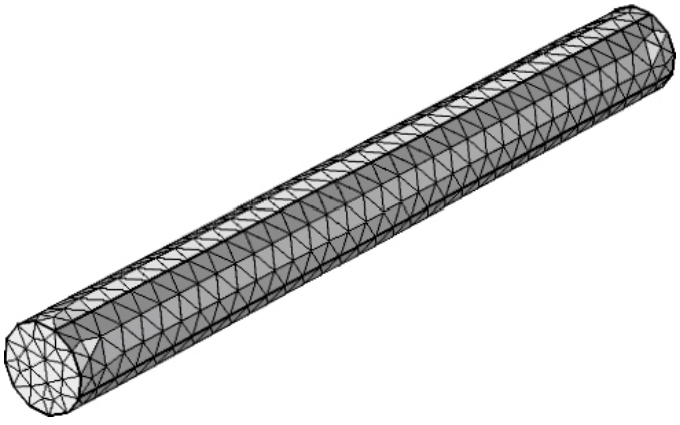

Figure A-1. *Finite element mesh used in the study in Comsol.*

[2] (http://www.thermochimie-tdb.com/).

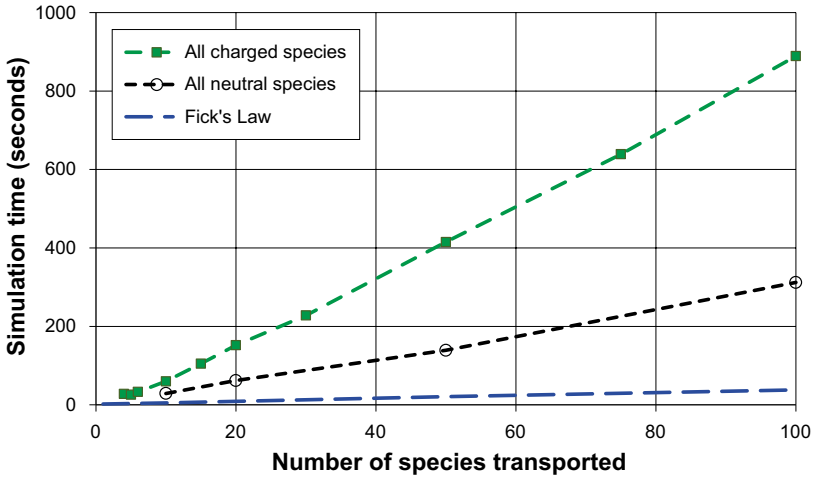

Figure A-2. *Results of the simulations using Comsol in terms of cpu times as a function of the number of species transported: (a) Fick's law, and Nernst-Planck equations using (b) all charged species and (c) all neutral species.*

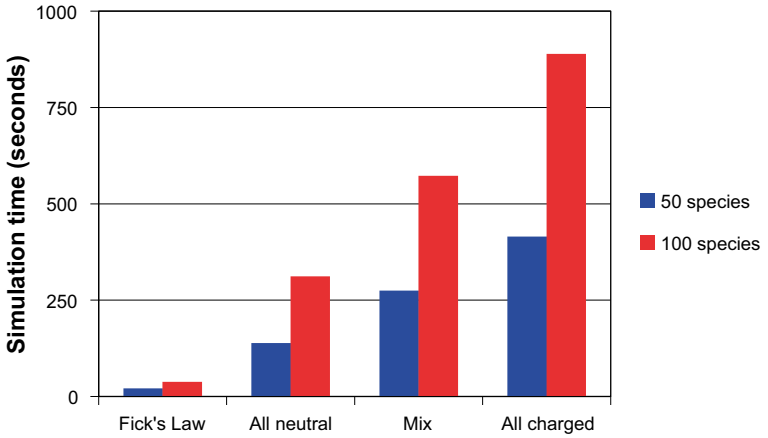

Figure A-3. *Results of the simulations using Comsol in terms of cpu times for 50 and 100 transported species: (a) Fick's law, and Nernst-Planck equations using (b) all neutral species, (c) a mix of charged and neutral species, and (d) all neutral species.*

Appendix B

Benchmark of multi-porosity diffusion model

In order to verify the implementation of the various features for multicomponent diffusion in clays that have been implemented in CrunchFlow and PhreeqC geochemical codes, a benchmark exercise has been conducted. These codes have been chosen because they are widely used and have been further developed with the special features needed to simulate ionic diffusion in compacted bentonite.

CrunchFlow and PhreeqC enable the calculation ionic reactive transport in bentonite and clays more accurately than other geochemical codes. In particular, these codes allow considering explicitly in the models the following features:

- Micro- (EDL) and macro-porosity (bulk or free water).
- Double layer (DL) and bulk solute concentrations using Donnan approximation.
- Electrochemical multispecies diffusion (Nernst-Planck equations) separately in EDL and bulk.
- Chemical reactions using standard equilibrium and/or kinetic formulations.

However, since the implementation of these features is recent in both codes and differ slightly between them, they need to be tested and compared in order to build confidence in their performance.

The benchmark consists of a simple test involving NaCl diffusion in Na-montmorillonite (Figure B-1). The sample has 53.5 mm long (discretized in 100 cells in both codes) and a porosity of 0.49. The diffusion coefficients used are summarized in Table B-1.

This verification exercise has required checking the input consistency between codes regarding for instance:

- Activity models (extended Debye-Hückel).
- Thermodynamic databases (LLNL).
- Protonation/deprotonation and Na complexation constants.
- Sorption sites concentrations (in units of mol/m^3 rock or mol/kgw).
- Solution charge balance.
- Surface complexation models excluding or including electrostatic terms.
- Diffusion coefficients.
- Surface equilibration mode.

Table B-1. Diffusion coefficients for the individual species used in the benchmark.

Diffusion coefficient (m^2/s)	
Default	1.50E−09
D_{Na+}	1.33E−09
D_{Cl-}	2.03E−09
D_{H+}	9.31E−09
D_{OH-}	5.27E−09

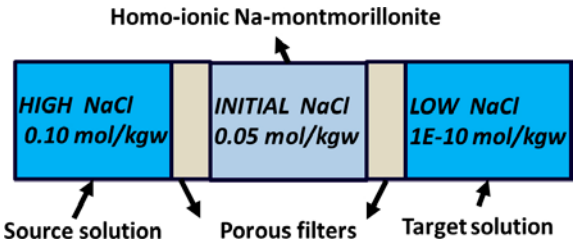

Figure B-1. *Setup of the benchmark simulation of NaCl diffusion in homo-ionic bentonite.*

Different calculation variants were considered in a stepwise manner to verify each feature separately:

- Nernst-Planck + dynamic porosity + Donnan equilibrium.
- Nernst-Planck + dynamic porosity + Donnan equilibrium + surface protonation.
- Nernst-Planck + dynamic porosity + Donnan equilibrium + surface protonation + surface complexation model.

Only the results of the most complex simulation are presented here. The porosity distribution of a CrunchFlow simulation in the case of multi-component diffusion (Nernst-Planck), dynamic porosity distribution, Donnan equilibrium, and surface reactions (protonation and Na^+ complexation) is shown in Figure B-2. It may be observed that the diffusion of ions from the upstream solution, with higher ionic strength than the sample pore water and downstream solution, induces an increase of the bulk porosity. This is due to the reduction of the Debye length at higher ionic strength (presented in Chapter 2).

The comparison of the porosity distribution between the two codes is shown in Figure B-3 for 0.5 and 10 days of diffusion, showing an excellent agreement. In turn, Na^+ in the bulk and micro porosities, and surface complexation of Na^+, are depicted in Figure B-4 and Figure B-5, also showing a remarkable agreement.

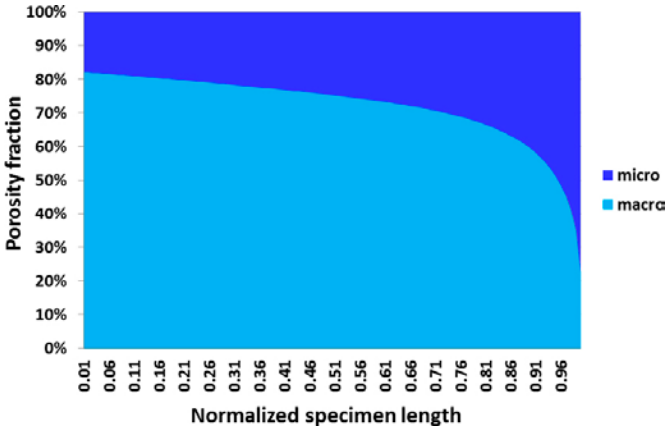

Figure B-2. *Profile of porosity distribution between micro and bulk across the normalized specimen length after 10 days of diffusion.*

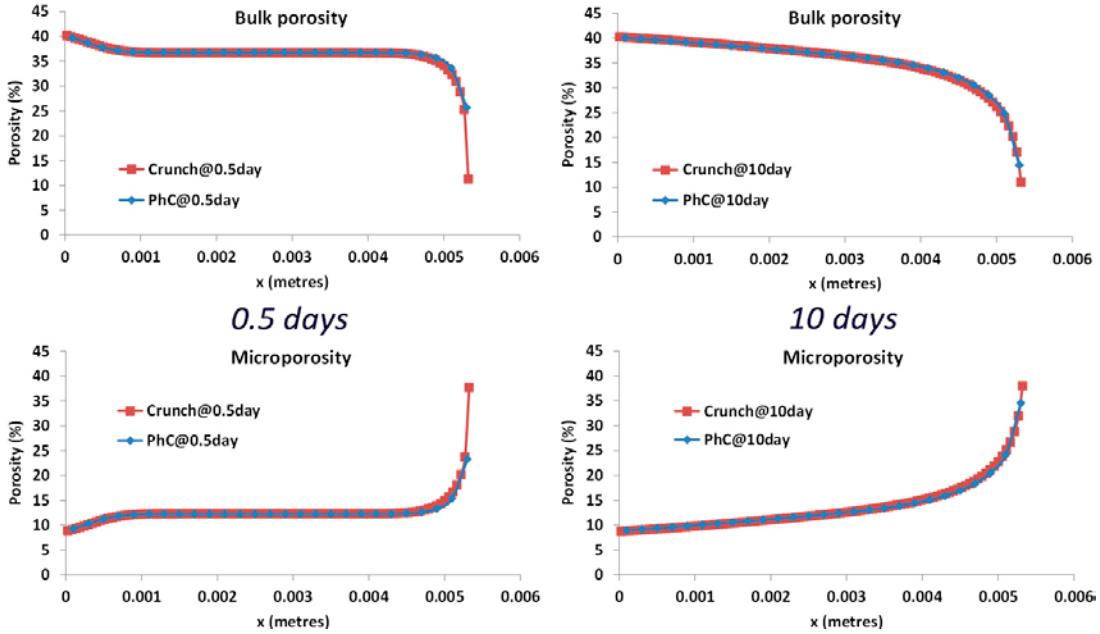

Figure B-3. *Comparison of profiles of porosity distribution between micro and bulk across the length after 0.5 and 10 days: CrunchFlow (Crunch) and PhreeqC (PhC).*

From the presented benchmarking exercise it may be concluded that:

- Multispecies electrochemical diffusion in a dual porosity medium (i.e. pure transport) yields closely matching results between the two codes both in the bulk and micro porosities.
- The results of the implemented dynamic porosity update in CrunchFlow compares very well to those obtained with PhreeqC.
- Dual porosity surface complexation in PhreeqC always includes the electrostatic terms, while CrunchFlow allows to choose either the electrostatic or non-electrostatic model.
- The above is important, as simple batch calculations yield dissimilar results when the electrostatic terms are included, which effect gets propagated into the 1D reactive transport simulation.

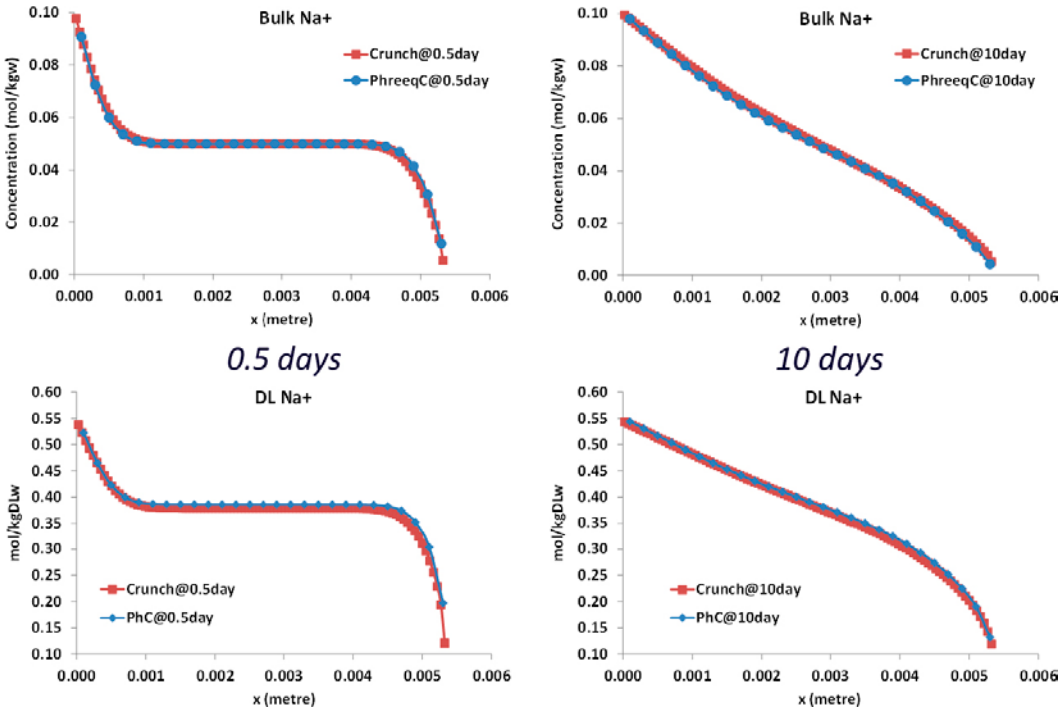

Figure B-4. *Profiles of Na^+ concentration in the micro (mol per kg of water in the DDL) and bulk (mol per kg of water in the bulk) porosities across the specimen length after 0.5 and 10 days: comparison between CrunchFlow (Crunch) and PhreeqC (PhC).*

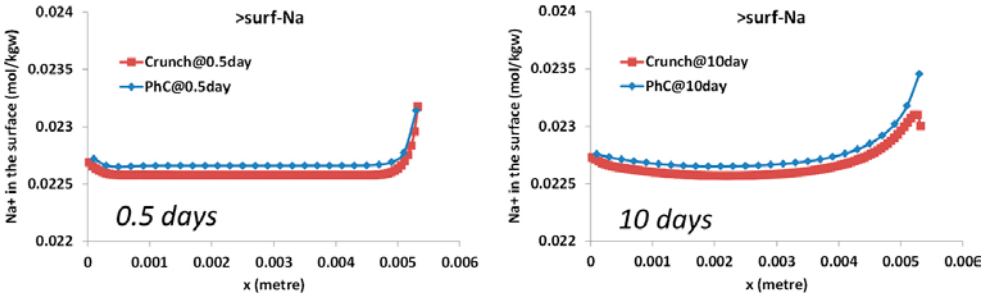

Figure B-5. *Profiles of Na^+ (mol/kgw) complexed in the surface of montmorillonite across the specimen length after 0.5 and 10 days: comparison between CrunchFlow (Crunch) and PhreeqC (PhC).*

Arkitektkopia AB, Bromma, 2016

SKB is tasked with managing Swedish nuclear and radioactive waste in a safe way.

skb.se